Loss of *Tifab*, a del(5q) MDS gene, alters hematopoiesis through derepression of Toll-like receptor–TRAF6 signaling

Melinda E. Varney,[1] Madeline Niederkorn,[1,2] Hiroyasu Konno,[3] Takayuki Matsumura,[3] Jin Gohda,[3] Nobuaki Yoshida,[4] Taishin Akiyama,[3] Susanne Christie,[1] Jing Fang,[1], David Miller,[1] Andres Jerez,[5] Aly Karsan,[6,7] Jaroslaw P. Maciejewski,[5] Ruhikanta A. Meetei,[1] Jun-ichiro Inoue,[3] and Daniel T. Starczynowski[1,8]

[1]Division of Experimental Hematology and Cancer Biology, Cincinnati Children's Hospital Medical Center, Cincinnati, OH 45229
[2]Department of Biological Sciences, University of Cincinnati, Cincinnati, OH 45267
[3]Division of Cellular and Molecular Biology, Department of Cancer Biology and [4]Laboratory of Developmental Genetics, Center for Experimental Medicine and Systems Biology, The Institute of Medical Science, the University of Tokyo, Shirokanedai, Minato-ku, Tokyo 108-8639, Japan
[5]Department of Translational Hematology and Oncology Research, Taussig Cancer Institute, Cleveland Clinic, Cleveland, OH
[6]Michael Smith Genome Sciences Centre and [7]Department of Pathology and Laboratory Medicine, BC Cancer Research Centre, Vancouver, BC V5Z 1L3, Canada
[8]Department of Cancer Biology, University of Cincinnati College of Medicine, Cincinnati, OH 45267

TRAF-interacting protein with forkhead-associated domain B (*TIFAB*) is a haploinsufficient gene in del(5q) myelodysplastic syndrome (MDS). Deletion of *Tifab* results in progressive bone marrow (BM) and blood defects, including skewed hematopoietic stem/progenitor cell (HSPC) proportions and altered myeloid differentiation. A subset of mice transplanted with *Tifab* knockout (KO) HSPCs develop a BM failure with neutrophil dysplasia and cytopenia. In competitive transplants, *Tifab* KO HSPCs are out-competed by wild-type (WT) cells, suggesting a cell-intrinsic defect. Gene expression analysis of *Tifab* KO HSPCs identified dysregulation of immune-related signatures, and hypersensitivity to TLR4 stimulation. TIFAB forms a complex with TRAF6, a mediator of immune signaling, and reduces TRAF6 protein stability by a lysosome-dependent mechanism. In contrast, *TIFAB* loss increases TRAF6 protein and the dynamic range of TLR4 signaling, contributing to ineffective hematopoiesis. Moreover, combined deletion of TIFAB and miR-146a, two genes associated with del(5q) MDS/AML, results in a cooperative increase in TRAF6 expression and hematopoietic dysfunction. Re-expression of TIFAB in del(5q) MDS/AML cells results in attenuated TLR4 signaling and reduced viability. These findings underscore the importance of efficient regulation of innate immune/TRAF6 signaling within HSPCs by TIFAB, and its cooperation with miR-146a as it relates to the pathogenesis of hematopoietic malignancies, such as del(5q) MDS/AML.

CORRESPONDENCE
Daniel T. Starczynowski:
Daniel.Starczynowski@cchmc.org

Abbreviations used: AML, acute myeloid leukemia: BMF, BM failure; BMT, BM transplant; cBMT, competitive BMT; CDR, commonly deleted region; HSC, hematopoietic stem cell; HET, heterozygous; HSPC, hematopoietic stem and progenitor cell; LSK, Lineage$^-$Sca1$^+$c-Kit$^+$; LT-HSC, long-term HSC; MDS, myelodysplastic syndrome; PB, peripheral blood; TIFAB, TRAF-interacting protein with forkhead-associated domain B.

Myelodysplastic syndrome (MDS) refers to a group of hematopoietic stem cell (HSC) disorders associated with ineffective hematopoiesis, blood cytopenias, myeloid dysplasia, genomic instability, and predisposition to acute myeloid leukemia (AML) or bone marrow failure (BMF). Recent classifications of MDS describe eight subtypes based on biological, genetic, and morphological features (Cazzola and Malcovati, 2010). Independent of classification, MDS is propagated by rare and defective HSCs, and is defined by recurring cytogenetic changes and somatic point mutations. The most common cytogenetic alteration in MDS is deletion of chromosome (chr) 5q (del(5q)). In the absence of other cytogenetic alterations, MDS patients with a del(5q) exhibit refractory anemia, neutropenia, and

The Rockefeller University Press $30.00
J. Exp. Med. 2015 Vol. 212 No. 11 1967–1985
www.jem.org/cgi/doi/10.1084/jem.20141898

elevated platelets associated with hypolobulated megakaryocytes (Giagounidis et al., 2006). Del(5q) is found in 25% of therapy-related MDS cases, which occur as a result of treatment with alkylating agents for unrelated conditions, and is strongly correlated with progression to AML (Haase et al., 2007; Haase, 2008; Qian et al., 2010). Although two commonly deleted regions (CDRs) have been mapped on chr 5q each spanning ∼1 Mb, a distal locus at 5q33.1, and a proximal locus at 5q31.1(Zhao et al., 1997), there are multiple genes that likely contribute to the pathogenesis of del(5q) MDS (Le Beau et al., 1989; Willman et al., 1993; Boultwood et al., 1994, 1997, 2000, 2002, 2007; Jaju et al., 1998). Clonal dominance of del(5q) cells is driven by haploid expression of CSNK1A1 (Schneider et al., 2014), whereas the erythroid defect has been attributed to *RPS14* genes located within the distal CDR (Ebert et al., 2008; Barlow et al., 2010). Thrombocytosis associated with megakaryocytic dysplasia, neutropenia, and clonal dominance, are caused by loss of two miRNAs, miR-145 and miR-146a, in del(5q) MDS patients (Kumar et al., 2009; Starczynowski et al., 2010). Germline knockout of mouse miR-146a results in an early onset of myeloid expansion in the BM, and progression to more aggressive diseases such as lymphomas, BMF, and myeloid leukemia (Lu et al., 2010; Boldin et al., 2011; Zhao et al., 2011). Furthermore, overexpression of TRAF6, a miR-146a target gene, in mouse HSPCs mimics certain hematopoietic defects observed in miR-146a–deficient mice, including neutropenia, dysplasia, and myeloid leukemia. Overexpression of TRAF6, however, also results in elevated platelets. Some of the effects are mediated by IL-6, as overexpression of TRAF6 in *Il6*-deficient HSPCs restores platelets and neutrophil counts. *DIAPH1*, which encodes mDia1, is located on 5q31.3, which resides between the two commonly deleted regions in del(5q) MDS. mDia1-deficient mice exhibit an age-dependent granulocytopenia, and myeloid dysplasia in the BM, in part through increased TLR4 signaling. The proximal CDR at 5q31.1 is associated with aggressive forms of del(5q) and includes ∼12 coding genes. Two of these genes, *CTNNA1* and *EGR1*, are thought to contribute to cell survival and myeloproliferation, respectively (Joslin et al., 2007; Liu et al., 2007). *HSPA9* and *PPP2CA* have also been implicated in aspects of the del(5q) MDS/AML phenotype. Despite this recent progress, detailed molecular, cellular, and genetic analyses of candidate genes on chr 5q are required to completely understand the pathogenesis of del(5q) MDS/AML.

Derepression of TRAF6, as a result of miR-146a haploinsufficiency, is one molecular consequence of del(5q) (Starczynowski et al., 2010; Boldin et al., 2011). TRAF6 is an E3 ubiquitin ligase and signal transducer of the innate immune signaling pathway in response to pathogens and host damage-associated molecules (Wu and Arron, 2003). A search of annotated genes within or near the CDR in del(5q) revealed a relatively uncharacterized gene, TRAF-interacting protein with forkhead-associated domain B (*TIFAB*). *TIFAB* resides within the proximal CDR on band 5q31.1, and belongs to a family of forkhead-associated domain proteins that also includes TIFA. TIFA was originally identified as a TRAF6-interacting protein in a yeast two-hybrid screen (Kanamori et al., 2002; Takatsuna et al., 2003), whereas TIFAB was identified as a TIFA-related protein by an in silico homology screen (Matsumura et al., 2004, 2009). To investigate whether loss of TIFAB is important to the pathophysiology of del(5q) MDS/AML, in this study, we characterized a germline *Tifab* knockout (KO) mouse. *Tifab*$^{-/-}$ mice exhibit progressive hematopoietic defects, including skewed HSPC proportions, altered myeloid differentiation, and a BMF-like disease associated with BM dysplasia and cytopenia. *Tifab*$^{-/-}$ BM cells are hypersensitive to Toll-like receptor 4 (TLR4) stimulation, suggesting that loss of TIFAB alters the innate immune pathway. Independent of *TRAF6* mRNA, TIFAB loss results in stabilization of TRAF6 protein. Moreover, combined deletion of TIFAB and miR-146a results in a cooperative increase in TRAF6 expression and hematopoietic dysfunction in vivo. This provides a potential molecular explanation for altered TLR4 sensitivity and the BMF phenotype. Collectively, our results provide evidence that deletion of TIFAB contributes to an MDS-like hematopoietic phenotype in mice by changing the dynamic range of the innate immune pathway in HSPCs through the regulation of TRAF6 protein stability.

RESULTS

TIFAB resides within the minimally deleted region on chromosome 5q in MDS and AML

Chronic innate immune signaling is associated with MDS HSPCs, partly due to deletion of miR-146a and DIAPH1. Given that the innate immune pathway is tightly regulated by negative feedback loops, we hypothesized that other genes on chr 5q cooperate to regulate this pathway. To identify such genes, we searched all annotated genes within or near the proximal and distal CDRs using the current assembly of the human genome (GRCh37/hg19), which revealed *TIFAB* (NM_001099221) on band 5q31.1 (chr5:134,784,560-134,788,089 bp; Fig. 1 A). The genomic location of *TIFAB* resides within the proximal CDR adjacent to *CXCL14* (Fig. 1 A; Le Beau et al., 1989). Previous studies have delineated the boundaries of the 5q31.1 CDR. Although the smallest reported interval spans ∼1.5 Mb (from 136.25 – 137.80 Mb; Zhao et al., 1997), boundaries extending from *IL-4* (132.00 Mb) to *UBE2D2* (139.01 Mb) are more commonly reported (Fig. 1 A; Le Beau et al., 1989, 1993). Cytogenetic data from The Cancer Genome Atlas (TCGA) confirms that chr 5q deletions in human AML encompass the *TIFAB* locus (Fig. 1 A). According to these findings, *TIFAB* is one of the genes that is deleted in nearly all reported cases of the aggressive subtypes of del(5q) MDS and AML. To determine whether TIFAB is a relevant candidate gene within the 5q31.1 CDR, we first examined the normal expression of *TIFAB* mRNA in HSPC populations from humans and mice. *TIFAB* mRNA is expressed highest in human CD34^{+} cells and the equivalent mouse Lineage-negative (Lin^{-}) BM cells (Fig. 1 B). To determine whether TIFAB mRNA is affected by del(5q) in MDS, we examined publically

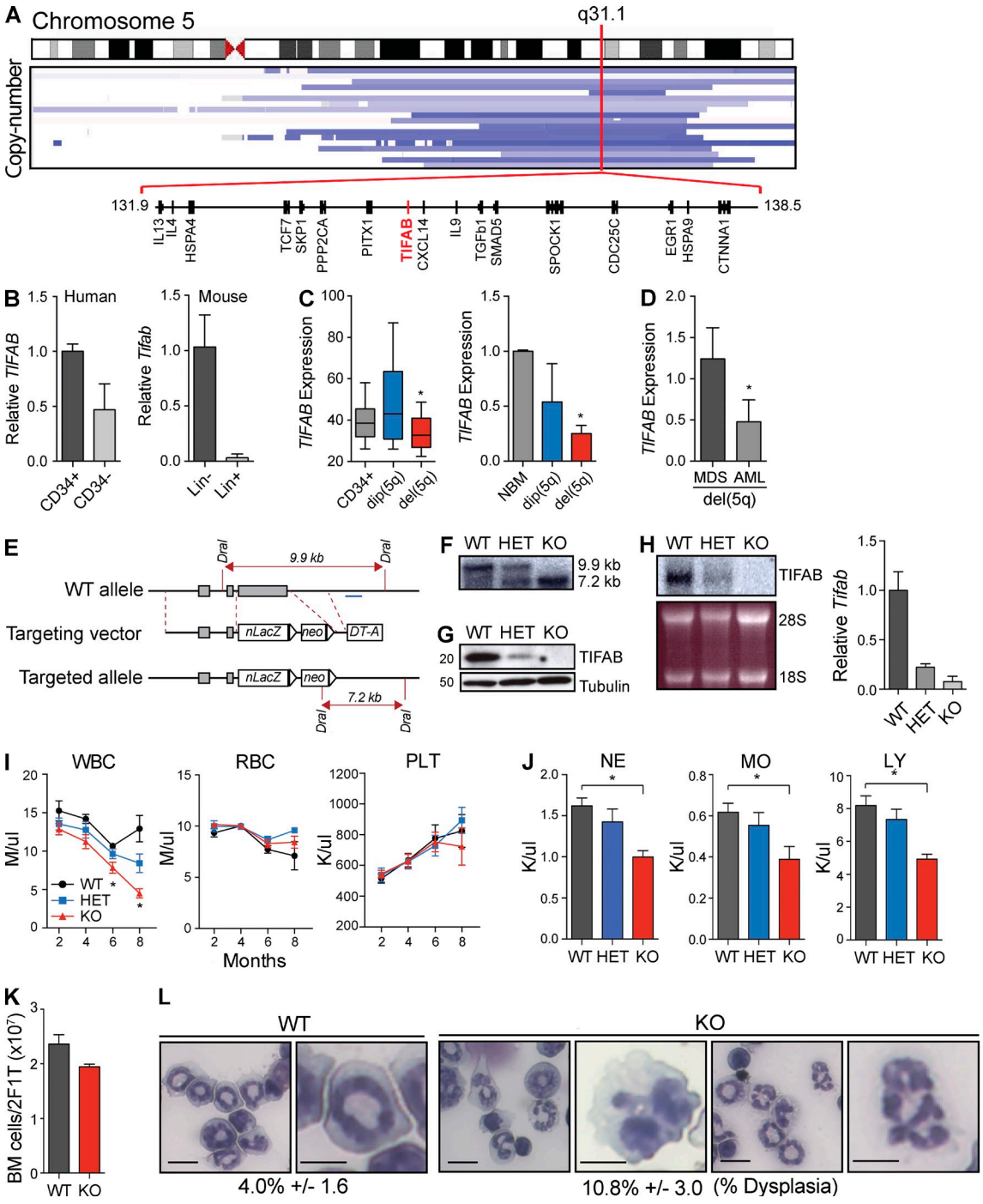

Figure 1. TIFAB deletion in del(5q) MDS/AML and mouse BM cells. (A) Schematic representation showing the genomic position of the TIFAB locus at chr 5q31.1. Below, blue/purple horizontal bars show extent of chr 5q deletions in human AML. (B) qPCR analysis of TIFAB mRNA in human CD34$^+$ and CD34$^-$ (left), and mouse lineage positive (Lin$^+$) and lineage negative (Lin$^-$; right) BM cells. (C) TIFAB mRNA expression in normal CD34$^+$ BM cells (n = 17), refractory anemia, and refractory anemia with excess blasts MDS CD34$^+$ cells with del(5q) (n = 47) or diploid 5q status (n = 127) adapted from public gene expression studies (Pellagatti et al., 2006; left). TIFAB mRNA expression was independently verified in normal, MDS dip(5q) (n = 4), and del(5q) (n = 4) BM mononuclear cells (right). *, $P < 0.05$; Student's t test. (D) TIFAB mRNA expression by qRT-PCR in MDS (n = 12) and AML (n = 4) mononuclear cells with del(5q). (E) Schematic representation of targeted *Tifab* allele. Exon 3, which contains the entire coding sequence, is deleted and replaced with a β-galactosidase and neomycin-resistant gene cassette floxed by loxP sites. The position of the 3′ probe for Southern blot is shown in blue. (F) 3′ Southern blot is shown to confirm germline deletion of *Tifab*. (G) Immunoblot analysis of BM lysates for TIFAB and tubulin protein expression from *Tifab*$^{+/+}$ (WT), *Tifab*$^{+/-}$ (HET), and *Tifab*$^{-/-}$ (KO) mice. (H) *Tifab* mRNA was determined by Northern blot analysis (left) and by qRT-PCR (right). (I) BM isolated from *Tifab* WT, HET, and KO mice was transplanted into lethally irradiated syngeneic recipient BoyJ mice. PB counts from mice transplanted with *Tifab* WT, HET, and

available gene expression data obtained from MDS CD34$^+$ patient samples (Pellagatti et al., 2006) and by qRT-PCR in an independent cohort of MDS patient samples. TIFAB mRNA was significantly lower in CD34$^+$ and BM mononuclear (MNC) cells isolated from MDS patients with del(5q) as compared with cells from MDS patients diploid at chr 5q (Fig. 1 C). Furthermore, *TIFAB* expression was significantly lower in del(5q) AML as compared with del(5q) MDS MNC (<60%; Fig. 1 D). These findings suggest that TIFAB may be a relevant gene in the pathogenesis of del(5q) MDS and/or AML.

Tifab deletion results in hematopoietic defects upon BM transplantation

To determine whether loss of TIFAB contributes to hematopoietic defects, we generated a constitutional knockout mouse model. The *Tifab* locus was targeted in embryonic stem cells with a construct containing LacZ in place of exon 3, which contains the entire coding sequence (Fig. 1 E). Germline deletion of the *Tifab* locus corresponded with loss of *Tifab* mRNA and protein (Fig. 1, F–H). Heterozygous (*Tifab*$^{+/-}$) and homozygous (*Tifab*$^{-/-}$) *Tifab*-deleted mice were born at expected Mendelian ratios and appeared physically normal. Peripheral blood (PB) counts at 6 and 12 mo of age were normal for all mice (unpublished data). Mature and immature BM cell populations of young or old *Tifab*-deficient (*Tifab*$^{+/-}$ and *Tifab*$^{-/-}$) mice, as well as spleen sizes, were indistinguishable from WT (*Tifab*$^{+/+}$) mice (unpublished data). However, a small subset of *Tifab*$^{-/-}$ and *Tifab*$^{+/-}$ mice, when aged beyond 1 yr, became moribund, presenting with enlarged spleens and evidence of BMF (cytopenia; unpublished data). Overall, these observations indicate that TIFAB is not required for steady-state hematopoiesis. To investigate the cell-autonomous function of *Tifab*-deficient HSPCs upon BM transplantation, BM cells from WT, *Tifab*$^{+/-}$, and *Tifab*$^{-/-}$ mice were transplanted into lethally radiated syngeneic recipient mice. Mice receiving *Tifab*-deficient BM exhibited a progressive decline in peripheral white blood cell (WBC) counts (4.5 K/µl vs. 12.9 K/µl; P = 0.0014), without changes in red blood cell or platelet counts (Fig. 1 I). At 6 mo after transplant, mice transplanted with *Tifab*$^{-/-}$ BM cells exhibited significant reduction in neutrophils (0.99 K/µl vs. 1.62 K/µl; P < 0.0001), lymphocytes (4.93 K/µl vs. 8.18 K/µl; P < 0.001), and monocytes (0.38 K/µl vs. 0.61 K/µl; P = 0.0043; Fig. 1 J). Mice transplanted with *Tifab*$^{-/-}$ BM cells had a normal/hypocellular BM (Fig. 1 K); however, they exhibited dysplastic hypersegmented neutrophils, consistent with a granulocyte defect (10.8 ± 3.0% vs. 4.0 ± 1.6%; P = 0.027; Fig. 1 L).

Mice transplanted with *Tifab*-deficient HSPCs develop a bone marrow failure–like disease

Given that mice transplanted with *Tifab*-deficient BM cells developed worsening cytopenias, the mice were aged beyond 1 yr to determine whether they progress to a hematologic disease. By 6 mo, a subset of mice transplanted with *Tifab*$^{-/-}$ BM cells became moribund, and within 16 mo, ∼40% of *Tifab*$^{-/-}$ mice (4/11 mice; P = 0.06), and 25% of *Tifab*$^{+-}$ mice (4/15 mice; P = 0.15) were moribund, whereas no control mice died (0/9; Fig. 2 A). Moribund *Tifab*-deficient mice had significantly lower WBC counts, including fewer neutrophils (0.95 K/µl vs. 3.85 K/µl; P = 0.013), monocytes (0.43 K/µl vs. 1.05 K/µl; P = 0.12), and lymphocytes (2.70 K/µl vs. 15.1 K/µl; P = 0.0001; Fig. 2 B). However, RBC counts, hematocrit, and platelet counts in moribund *Tifab*-deficient mice were comparable to age-matched control mice (Fig. 2 B). Moribund *Tifab*-deficient mice also had reduced BM cellularity (Fig. 2 C) and smaller spleens (Fig. 2 D) as compared with control mice, suggestive of declining hematopoietic function. Morphological examination of BM cells from moribund *Tifab*-deficient mice did not indicate consistent evidence of myeloid dysplasia (Fig. 2 C). PB, BM, and spleen analysis of moribund *Tifab*-deficient mice showed heterogeneous expansion or diminution of myeloid, lymphoid, and erythroid proportions, which also varied between moribund mice (Fig. 2, E–G). Despite the variation in cell proportions, moribund *Tifab*-deficient mice clearly displayed abnormal composition of mature myeloid, lymphoid, and erythroid cells in the PB and BM. Although PB cytopenia were observed in all mice at time of death, HSPC proportions of *Tifab*-deficient BM were maintained, suggesting, that the cytopenia was not simply a result of loss of HSCs (Fig. 2 H). Therefore, the progressive cytopenia and death of a subset of mice receiving *Tifab*-deficient BM cells suggests impaired HSPC function after loss of TIFAB.

TIFAB regulates HSPC function and myeloid differentiation

Because TIFAB deletion results in a progressive decline in hematopoietic function (Fig. 1) and in marrow failure (Fig. 2), we examined the consequences of TIFAB loss before overt disease. Although HSPC populations of nontransplanted *Tifab*-deficient (*Tifab*$^{+/-}$ and *Tifab*$^{-/-}$) mice were similar to WT mice (Fig. 3 A), after BMT, mice receiving *Tifab*$^{-/-}$ BM cells exhibited increased long-term HSCs (LT-HSC; P < 0.0001), lineage$^-$Sca1$^+$cKit$^+$ (LSK; P = 0.0036), and common myeloid progenitors (CMP; P = 0.018), whereas a reduction in megakaryocyte-erythroid progenitors was observed (MEP; P = 0.0058; Fig. 3 B). Although HPSC proportions significantly differed between WT and *Tifab*-deficient mice, the

KO BM cells at the indicated time points (months; $n > 9$ per group) from three independent transplants. *, P < 0.05; Student's *t* test. WBC, white blood cell; RBC, red blood cell; and PLT, platelet. (J) PB counts from mice transplanted with *Tifab* WT, HET, and KO BM cells at 6 mo after transplant ($n > 9$ per group) from three independent experiments. *, P < 0.05; Student's *t* test. NE, neutrophils; LY, lymphocytes; and MO, monocytes. (K) BM cellularity was determined for two femurs and one tibia (2F1T) for WT ($n = 3$) and KO ($n = 3$) mice. (L) Wright-Giemsa–stained BM cytospins from representative mice transplanted with *Tifab* WT, HET, and KO BM cells. Percent neutrophil dysplasia is shown for below the images for WT ($n = 3$) and KO ($n = 3$) BM cells. Bars show BM cytospins at low (20 µm) and high (7.5 µm) magnification. Error bars are mean ± SEM values.

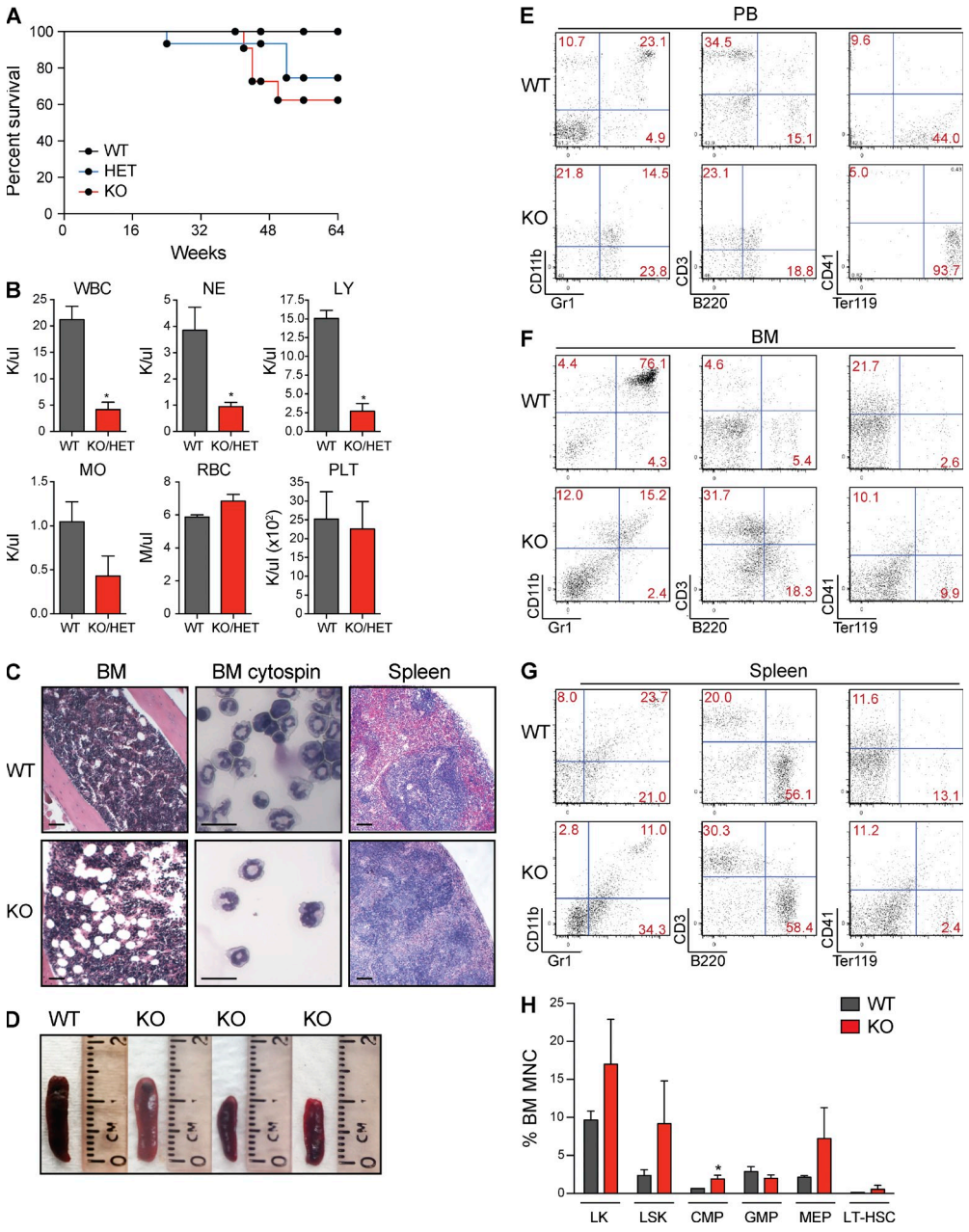

Figure 2. Transplantation of *Tifab*-deleted BM cells results in bone marrow failure. (A) Kaplan-Meier survival curves for transplanted mice reconstituted with *Tifab* WT ($n = 9$), HET ($n = 15$), or KO ($n = 11$) BM cells. Summary from three independent transplants. (B) PB counts from age-matched WT ($n = 3$) or moribund *Tifab* KO and HET ($n = 4$) mice. *, $P < 0.05$; Student's *t* test. WBC, white blood cell; RBC, red blood cell; PLT, platelet; NE, neutrophils; LY, lymphocytes; and MO, monocytes. (C) H&E-stained femur and spleen, and Wright-Giemsa–stained BM cytospins from a representative moribund *Tifab* KO mouse. Bars: (BM) 100 µm; (cytospins) 20 µm; (spleen) 100 µm. (D) Representative spleens from age-matched WT and moribund *Tifab* KO mice. (E–G) Flow cytometric analysis of PB (E), BM (F), and spleen (G) cells isolated from a WT and representative moribund *Tifab* KO transplant mouse. (H) Flow cytometric analysis of HSPC proportions in the BM of *Tifab* WT ($n = 3$) and moribund KO ($n = 2$) transplanted mice. Error bars are mean ± SEM values. *, $P < 0.05$.

proportion of mature BM cells was similar between WT and *Tifab*$^{-/-}$ transplanted mice (Fig. 3 C). However, the production of Gr1^{+} myeloid cells in the PB was significantly increased in mice transplanted with *Tifab*$^{-/-}$ BM cells ($P = 0.037$; Fig. 3 D). To assess whether TIFAB is important for hematopoietic progenitor differentiation in vitro, LSK isolated from WT or *Tifab*-deficient (*Tifab*$^{+/-}$ and *Tifab*$^{-/-}$) mice were examined for progenitor colony formation in methylcellulose. LSK from *Tifab*-deficient mice formed ∼50% more CFU-G colonies as compared with WT LSK ($P = 0.009$; Fig. 3 E), underscoring a functional defect in *Tifab*-deficient HSPCs and consistent with a role of TIFAB in myeloid differentiation.

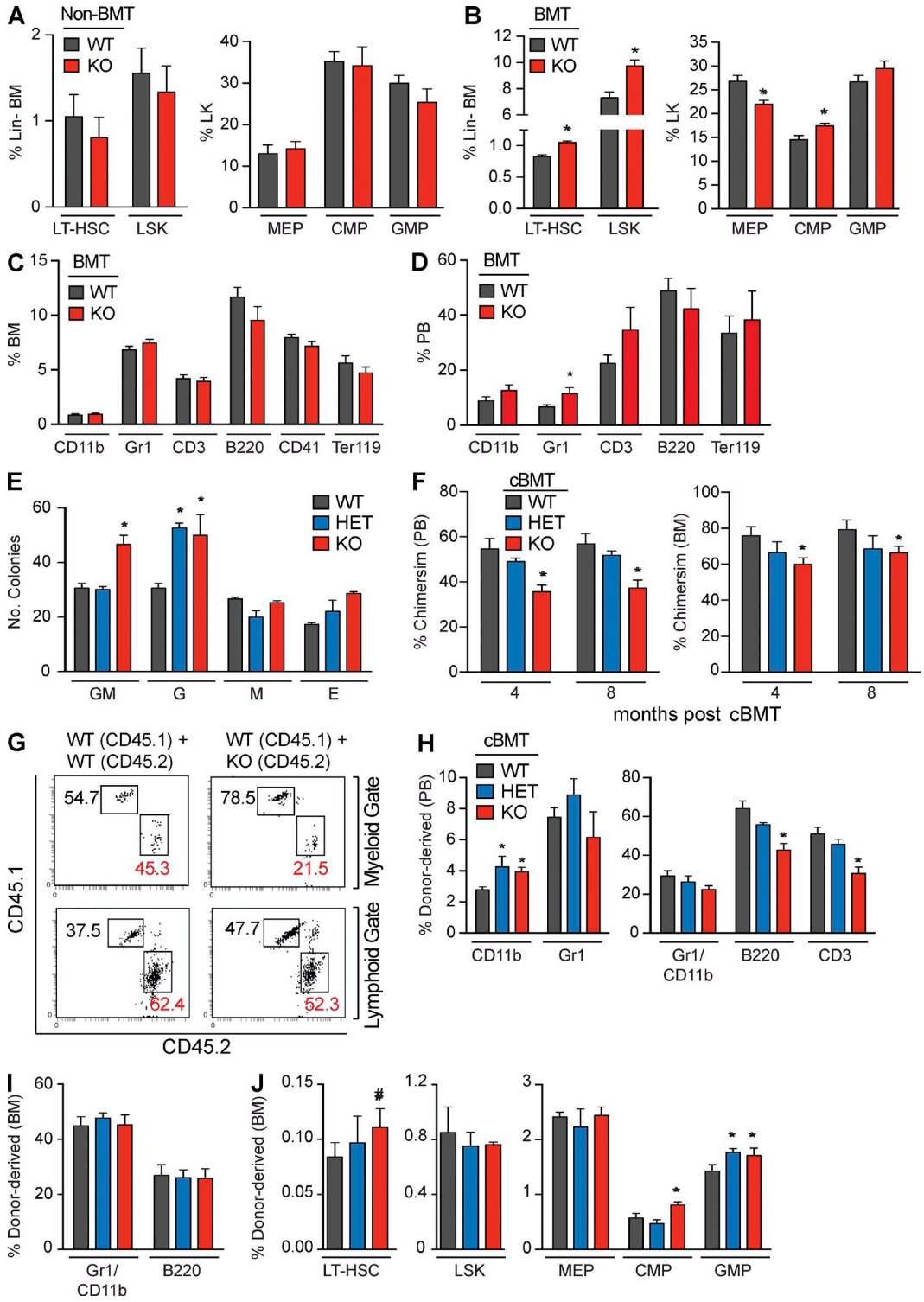

Figure 3. ***Tifab*$^{-/-}$ BM cells exhibit altered hematopoietic proportions after transplantation.** (A) LSK, LT-HSC (LSK^{+} CD150^{+}CD48^{-}), MEP, CMP, and GMP in BM cells from *Tifab* WT or KO mice ($n = 7$). (B) LSK, LT-HSC (LSK^{+} CD150^{+}CD48^{-}), MEP, CMP, and GMP in BM from mice transplanted with *Tifab* WT or KO BM cells from two independent experiments ($n = 6$). *, $P < 0.05$; Student's *t* test. (C and D) BM (C) and PB (D) proportions from mice transplanted with *Tifab* WT or KO BM cells ($n = 6$) from three independent experiments. *, $P < 0.05$; Student's *t* test. (E) Numbers of colony-forming cells in methylcellulose from LSK cells from *Tifab* WT, HET, or KO BM mice ($n = 6$; 2 independent BMT). *, $P < 0.05$; Student's *t* test. GM, granulocyte-monocyte; G, granulocyte; M, monocyte; E, erythroid (BFU-E). (F) 3×10^5 BM isolated from *Tifab* WT, HET, and KO mice (CD45.2) were mixed with equal numbers of competitor BoyJ BM cells (CD45.1), and then transplanted into lethally radiated syngeneic recipient BoyJ mice (CD45.1). PB and BM chimerism was

Competitive repopulation assays were performed to determine whether loss of *Tifab* affects HSPC function in vivo. Whole BM cells (3×10^5) from 8-wk-old CD45.2 WT, *Tifab*$^{+/-}$, or *Tifab*$^{-/-}$ mice were transplanted with equal numbers of 8-wk-old CD45.1 competitor BM cells into lethally irradiated CD45.1 recipient mice. PB chimerism was evaluated for 50 wk and was calculated based on the proportion of CD45.2 mononuclear cells (CD45.2/[CD45.2$^+$CD45.1]). Consistent with the persistent cytopenias after transplantation of *Tifab*-deficient BM cells, we observed a reduction in hematopoietic repopulation within the BM and PB, indicating that *Tifab*$^{-/-}$ HSPCs have a significant disadvantage in competitive transplantation and/or homing (Fig. 3 F). Lower chimerism of *Tifab*-deficient cells was caused by a reduction in lymphoid (CD3$^+$ and B220$^+$) and myeloid (CD11b$^+$ and Gr1$^+$) contribution to the PB (Fig. 3 G). To gain insight into the effects of TIFAB deletion on hematopoietic differentiation, donor-derived (CD45.2-positive) proportions were evaluated in the BM and PB from the competitive transplantation experiments. *Tifab* deficiency contributes to increased myeloid (CD11b$^+$; P = 0.015) and reduced lymphoid (B220$^+$ and CD3$^+$; P = 0.004) donor-derived proportions in the PB (Fig. 3 H), with minor consequences on myeloid and lymphoid donor-derived proportions in the BM (Fig. 3 I). In addition, donor-derived *Tifab*$^{-/-}$ cells resulted in increased CMP (P = 0.03), and slightly elevated LT-HSCs (P = 0.09) and GMP (P = 0.08) proportions (Fig. 3 J). The hematopoietic differences within mice competitively transplanted with *Tifab*$^{+/-}$ BM cells were consistent by some measures with that of *Tifab*$^{-/-}$-transplanted mice for CD11b-expansion and lymphoid-reduction in the PB (Fig. 3 H), and for expansion of the GMP compartment in the BM (Fig. 3 J). These findings suggest that *Tifab* deficiency affects myeloid/lymphoid-lineage differentiation and HSPC function, before development of overt hematologic disease consistent with BMF.

TIFAB regulates immune and survival gene signatures in HSPCs

To understand the molecular basis for impaired HSPC function and BMF after TIFAB deletion, we performed an expression analysis on sorted LSK isolated from 3-mo-old mice transplanted with WT or *Tifab*$^{-/-}$ BM cells ($n = 3$ mice/group). We selected this time point to capture the gene expression profile of *Tifab*$^{-/-}$ LSK after engraftment but before overt hematopoietic failure. Complete blood counts before isolation of LSK cells confirmed absence of BMF in all mice. Analysis of the gene expression data identified differentially expressed genes in *Tifab*$^{-/-}$ LSK cells, including 32 up-regulated (>1.7-fold) and 22 down-regulated (<1.7-fold; Fig. 4 A and Table S1). To elucidate the relevant signaling pathway regulated after *Tifab* loss in HSPCs, we performed a gene set enrichment analysis (GSEA; Subramanian et al., 2005), which revealed overexpression of immune and infection response signatures, particularly related to interferon-regulated genes (Fig. 4 B). Down-regulated gene signatures in *Tifab*$^{-/-}$ LSK also included immune response signatures, but these were related to enterotoxin and LPS (Fig. 4, A and B). Interestingly, the immune-related gene signatures show a clear disparity between various immune insults, in which certain signatures (i.e., viral and interferon) are enriched, whereas other signatures (i.e., TNF and endo/enterotoxin) are down-regulated. Select genes from the microarray analysis that were overexpressed (*Il6* and *Bcl2a1*) and down-regulated (*Tnfaip3* and *Sod2*) in *Tifab*$^{-/-}$ LSK were confirmed by qRT-PCR (Fig. 4 C).

Although dysregulation of immune gene signatures is evident even in resting *Tifab*$^{-/-}$ HPSC, these findings prompted us to examine the role of TIFAB in regulating inducible gene expression. We selected two stimuli (TNF and LPS) that are associated with enriched GSEA signatures in *Tifab*-deficient HSPCs (Fig. 4 B). BM mononuclear cells (MNC) from WT and *Tifab*$^{-/-}$ mice were stimulated with TNF (10 ng/ml) or LPS (100 ng/ml) at various time points (0, 1, and 4 h) and examined for target gene expression by qRT-PCR. As expected, stimulation of WT BM cells with either LPS or TNF resulted in a time-dependent increase in *Il6*, *Bcl2a1*, *Tnfaip3*, and *Sod2* expression (Fig. 4, D and E). Although expression of certain genes was higher (*Il6* and *Bcl2a1*) or lower (*Tnfaip3* and *Sod2*) in *Tifab*$^{-/-}$ than WT BM cells at basal levels, LPS stimulation resulted in a significant and acute increase of all genes examined in *Tifab*$^{-/-}$ BM cells (Fig. 4 D). In contrast, TNF stimulation of *Tifab*$^{-/-}$ BM cells resulted in a delayed response of *Tnfaip3* and *Sod2*, and no dramatic differences of *Il6* and *Bcl2a1* expression (Fig. 4 E). These findings reveal that TIFAB controls the dynamic range of immune pathway activation downstream of TLRs, but not the TNF receptor (TNFR).

TIFAB forms a complex with TRAF6 and inhibits NF-κB

The molecular function of TIFAB that restricts immune signaling in MDS/AML remains to be determined. To uncover the molecular function of TIFAB, we performed a global proteome analysis to identify TIFAB-associated cofactors in a del(5q) leukemic cell line. We generated stable HL60 lines expressing human TIFAB tagged with both FLAG and HA epitopes. TIFAB and its associated partners were purified from total cell lysates derived from HL60 cells using tandem affinity immunoprecipitation, as previously described (Singh et al., 2008;

determined at 4 and 8 mo after transplantation. Calculated chimerism is based on the ratio of CD45.1 and CD45.2 mononuclear cells. Three independent experiments were performed. (G) Representative flow cytometric blots of PB chimerism at 8 mo after transplantation on myeloid (Gr1$^+$CD11b$^-$) and lymphoid (B220$^+$) gated populations. (H and I) Flow cytometric analysis of myeloid (CD11b and Gr1), and lymphoid (CD3 and B220) donor-derived CD45.2$^+$ proportions within the PB (H) and BM (I) of *Tifab* WT ($n = 4$), HET ($n = 4$), and KO ($n = 5$) competitively transplanted mice. *, P < 0.05; Student's *t* test. (J) Flow cytometric analysis of HSPC donor-derived CD45.2$^+$ proportions within the BM of *Tifab* WT ($n = 4$), HET ($n = 4$), and KO ($n = 5$) competitively transplanted mice at 8 mo. *, P < 0.05; Student's *t* test and Mann-Whitney test. Error bars are mean ± SEM values.

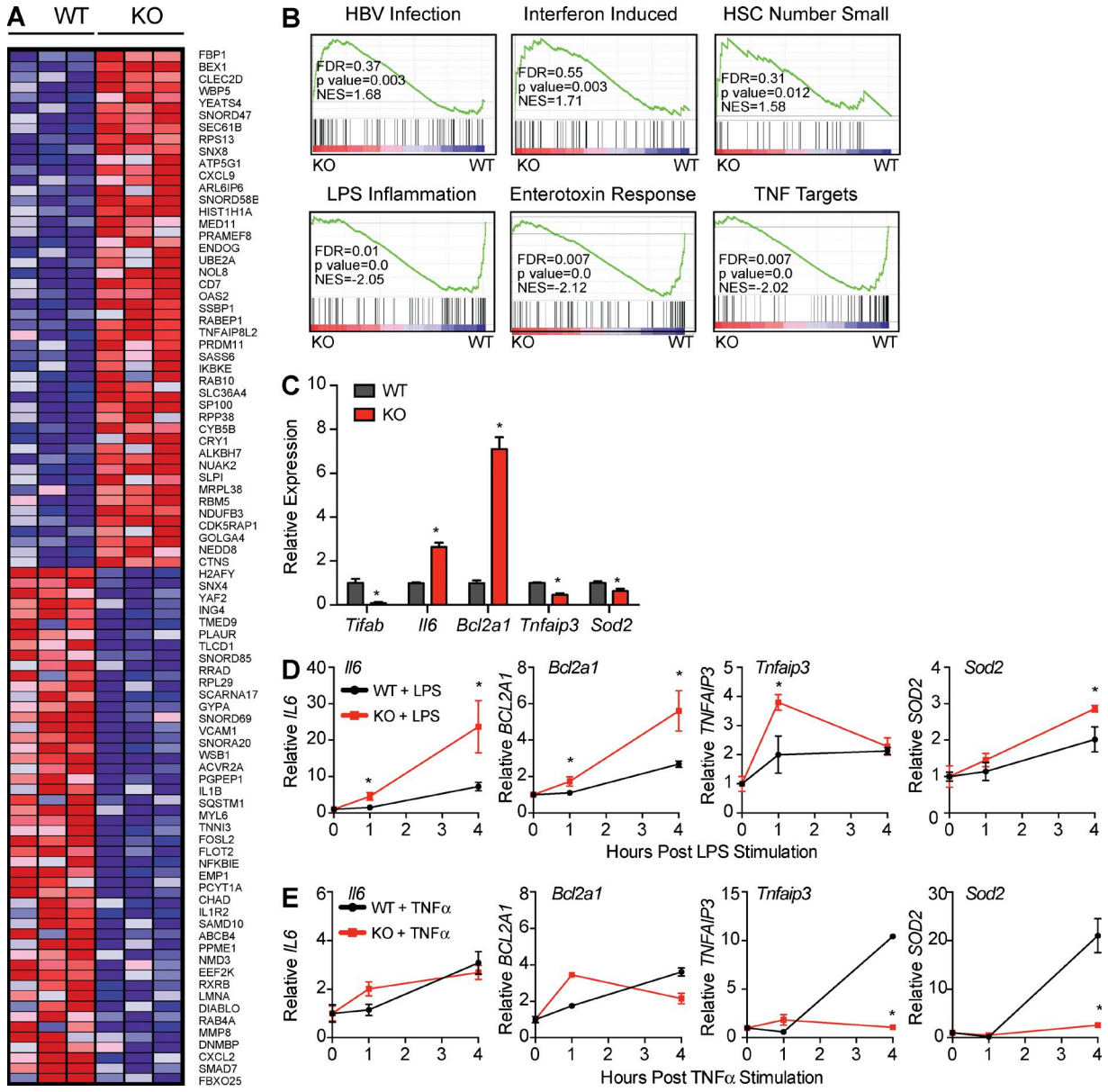

Figure 4. TIFAB suppresses immune signaling and NF-κB activation downstream of the TLR4 receptor in BM HSPCs. (A) Heat map generated from gene set enrichment analysis (GSEA) showing gene expression differences in LSK isolated from 3-mo-old mice transplanted with *Tifab* WT or KO BM cells ($n = 3$ mice/group). (B) GSEA of statistically significant gene sets enriched in the LSK cells of transplanted *Tifab*$^{-/-}$ cells (up in KO) or WT cells (down in KO). (C) Validation of gene expression of the indicated genes in BM MNC by qRT-PCR. *, $P < 0.05$; Student's *t* test. (D and E) Expression analysis of the indicated genes in BM MNC by qRT-PCR after stimulation with LPS (D; 100 ng/ml) or TNF (E; 10 ng/ml) for the indicated time points. Expression was normalized to time 0 (1.0). *, $P < 0.05$; Student's *t* test.

Fig. 5 A). Mass spectrometry (MS) analysis identified ∼300 unique protein partners of TIFAB. An MS-identified partner of TIFAB is TRAF6, a major component of the TLR signaling pathway and a functionally relevant protein in the pathogenesis of MDS/AML. Other TLR pathway molecules were also uncovered: SQSTM1/p62 and TIFA. To further investigate the TIFAB–TRAF6 interaction, HL60 cells expressing TIFAB were fractionated into cytoplasmic and nuclear fractions. The TIFAB–TRAF6 complex is formed predominantly within the cytoplasm (Fig. 5 B), which is consistent with the known role of TRAF6 signaling during TLR activation. TIFAB (double tagged with FLAG and HA) was also cotransfected with TRAF6 (tagged with FLAG) into HEK293 cells, and immunoprecipitated (anti-HA). In support of the MS analysis, immunoblotting of TRAF6 (anti-FLAG) confirmed that TIFAB co-immunoprecipitates with TRAF6 (Fig. 5 C).

Stimulation of TLRs mediates signals to several transcription factors, one of which is the NF-κB family. Because TIFAB

expression is low in THP1 and HL60 cells, whereas NF-κB activation is high, we first determined the consequences of TIFAB reexpression on NF-κB signaling in these relevant human cells. THP1 and HL60 cells were transduced with a vector encoding TIFAB or control (empty vector), and examined for phosphorylated IKKβ (pIKKβ), an indication of NF-κB activation. Overexpression of TIFAB resulted in significant reduction in pIKKβ, indicating that TIFAB reexpression is sufficient to inhibit NF-κB (Fig. 5 D). Because TLR and TNF receptor 2 (TNFR2) use different signaling mediators to activate NF-κB (Fig. 5 E), we wanted to determine the precise step at which TIFAB regulates receptor-induced NF-κB signaling. To examine this mechanism, we performed κB-site containing reporter assays transfected with various activators of NF-κB (IKKβ, RelA/p65) and ones downstream of TLR4 (TRAF6) or TNFR2 (TRAF2; Fig. 5 E). Co-transfection of TIFAB did not suppress IKKβ- (Fig. 5 F) or p65-mediated (Fig. 5 G) κB-site luciferase activity, indicating that TIFAB inhibits NF-κB signaling upstream of the NF-κB kinase complex (IKK) and its transcription factor (RelA/p65). However,

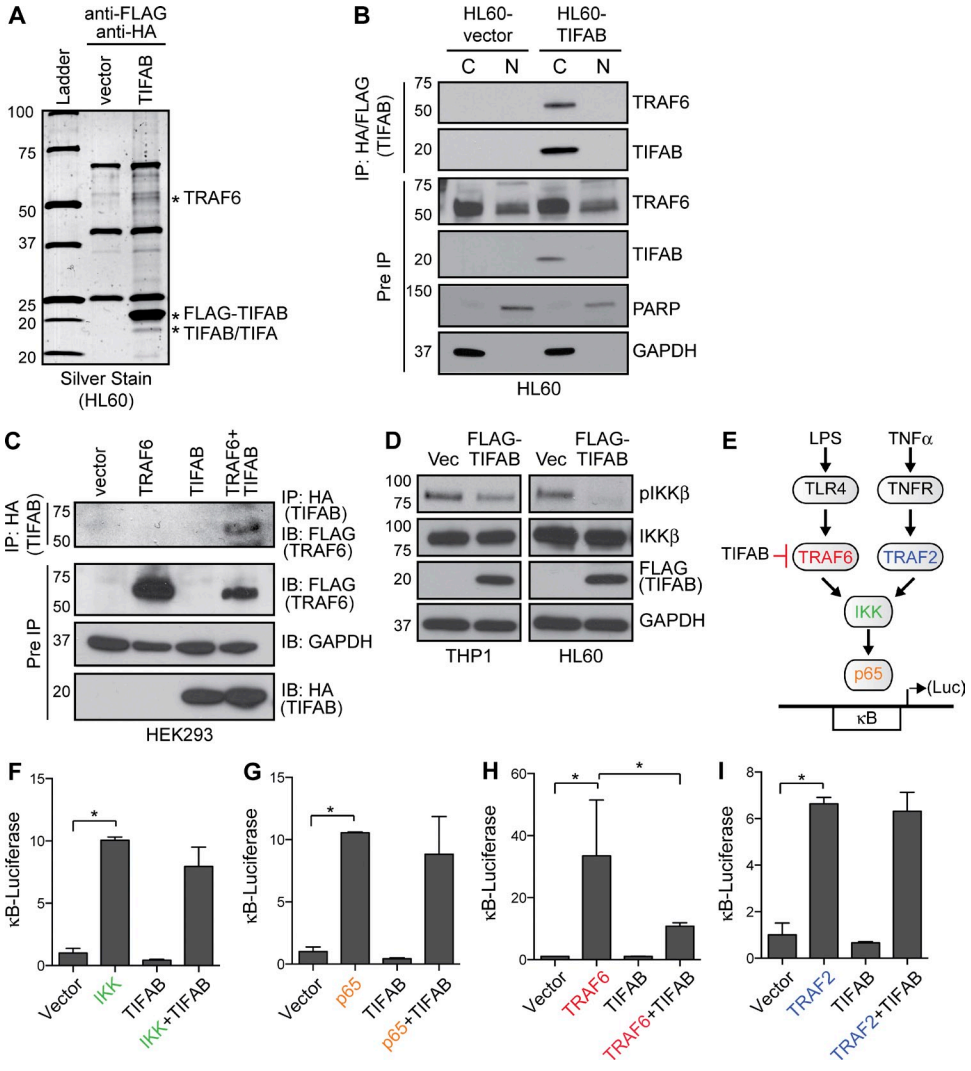

Figure 5. TIFAB binds to TRAF6 and suppresses NF-κB activation. (A) A representative silver stain after tandem affinity purification of FLAG-HA-TIFAB from HL60 cells. (B) TIFAB-expressing HL60 cells were lysed and fractionated into cytoplasmic (C) and nuclear (N) fractions, which were then subjected to coimmunoprecipitation of FLAG-HA-TIFAB. Immunoblotting for TRAF6, TIFAB, PARP (nuclear loading control), and GAPDH (cytosolic loading control) is shown. (C) Coimmunoprecipitation analysis of HEK293 transfected with empty vector, HA-TIFAB, FLAG-TRAF6, or HA-TIFAB and FLAG-TRAF6. Lysates were immunoprecipitated with anti-HA (TIFAB), and then blotted for FLAG (TRAF6). (D) Immunoblot analysis of THP1 and HL60 cells transduced with empty vector (Vec) or FLAG-TIFAB for phosphorylated IKKβ (pIKKβ), total IKKβ, and GAPDH. (E) Overview of TLR4 and TNFR-mediated activation of NF-κB, and the proposed regulation by TIFAB. (F–I) NF-κB activation was measured by κB-site containing reporter assays in HEK293 cells transfected with empty vector, TIFAB, and/or IKKβ (F), p65 (G), TRAF6 (H), or TRAF2 (I). Values are normalized to Renilla-luciferase and empty vector (1.0). Summary of three independent experiments. Error bars are mean ± SEM values. *, $P < 0.05$; Student's *t* test.

co-transfection of TIFAB significantly repressed κB-site luciferase activity by TRAF6 (Fig. 5 H). In contrast, TIFAB did not repress κB-site activation after transfection of TRAF2, a functionally related paralog of TRAF6 (Fig. 5 I). TIFAB represses TRAF6-, but not TRAF2-mediated NF-κB activation, implying that TIFAB selectively inhibits TLR/TRAF6-dependent NF-κB stimuli while having no effect on TNFR2/TRAF2-dependent NF-κB stimuli.

TIFAB restricts TLR activation by destabilizing TRAF6 protein

To investigate the mechanism by which TIFAB inhibits TRAF6-mediated signaling, we overexpressed TIFAB in HEK293 or HL60 cells. We observed reduced levels of transfected (HEK293: 60% decrease) and endogenous (HL60: 40% decrease) TRAF6 protein (Fig. 6 A). Moreover, expression of TIFAB reduced levels of cotransfected TRAF6, whereas the levels of TRAF2 were not affected (Fig. 6 B). Conversely, THP1 cells after knockdown of TIFAB (Fig. 6 C), as well as *Tifab*$^{-/-}$ BM cells after BM transplantation (Fig. 6 D), exhibited increased expression of TRAF6 protein. The effects of TIFAB on TRAF6 protein are independent of *TRAF6* mRNA, as overexpression of TIFAB did not reduce *TRAF6* mRNA in HEK293 cells (Fig. 6 E), nor did *Tifab* deficiency increase *Traf6* mRNA in BM cells (Fig. 6 F). To explore the possibility that TIFAB induces TRAF6 protein degradation, we used selective inhibitors of the proteasome (MG-132) or lysosome (3-MA). Treatment of HEK293 cells expressing TRAF6 and TIFAB with MG-132 did not restore TRAF6 protein levels (Fig. 6 G), indicating that TIFAB-mediated degradation of TRAF6 does not occur through the ubiquitin–proteasome pathway (Fig. 6 H). However, treatment with 3-MA partially restored TRAF6 protein expression in TIFAB-expressing HEK293 cells (Fig. 6 G), suggesting that TIFAB-mediated degradation may occur through the lysosome–autophagy pathway (Fig. 6 H).

TRAF6 is required for the hyperimmune response in Tifab-deficient hematopoietic cells

To establish whether *Tifab*-deficient BM cells exhibit increased LPS-response through TRAF6, rescue experiments were performed by depleting *Traf6* in *Tifab*$^{-/-}$ BM cells. WT and *Tifab*$^{-/-}$ BM cells were transduced with shTraf6 (shT6) or control shRNA (shCTL; Fig. 6 I), and then stimulated with LPS for up to 4 h. As in Fig. 4 D, LPS stimulation of WT BM cells expressing the control shRNA exhibited an increase in *Tnfaip3* and *Sod2* expression, whereas *Tifab*$^{-/-}$ BM stimulated with LPS exhibited a further increase in both *Tnfaip3* and *Sod2* levels (Fig. 6, J and K). Knockdown of *Traf6* in both WT and *Tifab*$^{-/-}$ BM cells completely abolished LPS-induced expression of *Tnfaip3* and *Sod2* (Fig. 6, J and K). Collectively, these findings have uncovered that TIFAB controls TLR signaling by binding and regulating TRAF6 protein stability through lysosomal degradation, but does not affect TNFR–TRAF2 signaling.

TIFAB and miR-146a cooperate to regulate TRAF6 expression and myeloid cell differentiation

Human miR-146a and TIFAB both reside on chr 5q and are co-deleted in ∼80% of del(5q) MDS and AML (Gondek et al., 2008). miR-146a$^{-/-}$ mice develop BMF and myeloid leukemia, in part because of derepression of TRAF6 mRNA and protein (Lu et al., 2010; Boldin et al., 2011; Zhao et al., 2011). Given that TIFAB and miR-146a are codeleted in MDS/AML, we examined whether there is a functional cooperation between TIFAB and miR-146a. miR-146a inhibits TRAF6 protein expression and reduces its mRNA levels, whereas herein we report that TIFAB inhibits TRAF6 by destabilizing its protein. Because miR-146a is an NF-κB target gene responsive to LPS, miR-146a expression was investigated in TIFAB-deficient BM cells. At basal levels and after LPS stimulation, miR-146a expression is significantly elevated in *Tifab*$^{-/-}$ BM MNC (2-fold and 15-fold at baseline and after stimulation, respectively; Fig. 7 A). Although TRAF6 protein is stabilized after BM transplantation in *Tifab*$^{-/-}$ BM cells (Fig. 6 D), *Traf6* mRNA is significantly reduced in *Tifab*$^{-/-}$ BM cells as compared with WT cells (Fig. 6 F and Fig. 7 B), suggesting that increased miR-146a expression in *Tifab*-deficient cells may suppress TRAF6 mRNA. To examine a cooperative effect of TIFAB and miR-146a deficiency on TRAF6 mRNA and protein expression, we generated double *Tifab*- and miR-146a–deficient mice. Combined deletion of *Tifab* and miR-146a restored TRAF6 mRNA expression to WT levels (Fig. 7 B). In addition, TRAF6 protein expression was synergistically increased in BM MNC from *Tifab*$^{-/-}$;miR-146a$^{-/-}$ mice (dKO) after BM transplantation as compared with single-knockout BM cells (Fig. 7 C). Collectively, miR-146a and TIFAB cooperate to suppress TRAF6 mRNA and protein expression in BM HSPCs.

To assess whether TIFAB and miR-146a cooperate to regulate hematopoietic progenitor differentiation in vitro, BM HSPCs isolated from WT, *Tifab*$^{-/-}$, miR-146a$^{-/-}$, or dKO mice were examined for progenitor colony formation in methylcellulose. Total colony formation was increased in dKO as compared with the single KO mice (Fig. 7 D). In addition, combined deletion of TIFAB and miR-146a resulted in an additive increase in CFU-G colony formation ($P = 0.007$), underscoring a functional cooperation between TIFAB and miR-146a during myeloid differentiation (Fig. 7 E). To determine whether combined deletion of TIFAB and miR-146a accentuates the cytopenia in vivo, BM cells from WT, *Tifab*$^{-/-}$, *miR-146*$^{-/-}$, and dKO mice were transplanted into lethally radiated syngeneic recipient mice. Mice reconstituted with *Tifab*-deficient BM exhibited a decline in peripheral neutrophils (2.1 vs. 3.0 K/μl; $P = 0.014$), lymphocytes (10.5 vs. 13.0 K/μl; $P < 0.006$), and RBCs (9.5 vs. 10.5 K/μl; $P = 0.01$) by 4 mo. Deletion of miR-146a had only minor effects on neutrophil ($P = 0.08$), lymphocyte ($P = 0.45$), or RBC ($P = 0.012$) counts (Fig. 7 F). In contrast, combined deletion of TIFAB and miR-146a resulted in a cooperative decrease in peripheral neutrophil (1.3 vs. 3.0 K/μl; $P < 0.0001$) and lymphocyte (7.5 vs. 13.0 K/μl; $P < 0.0001$) production, while not contributing further to RBC defects during the same time period (Fig. 7 F).

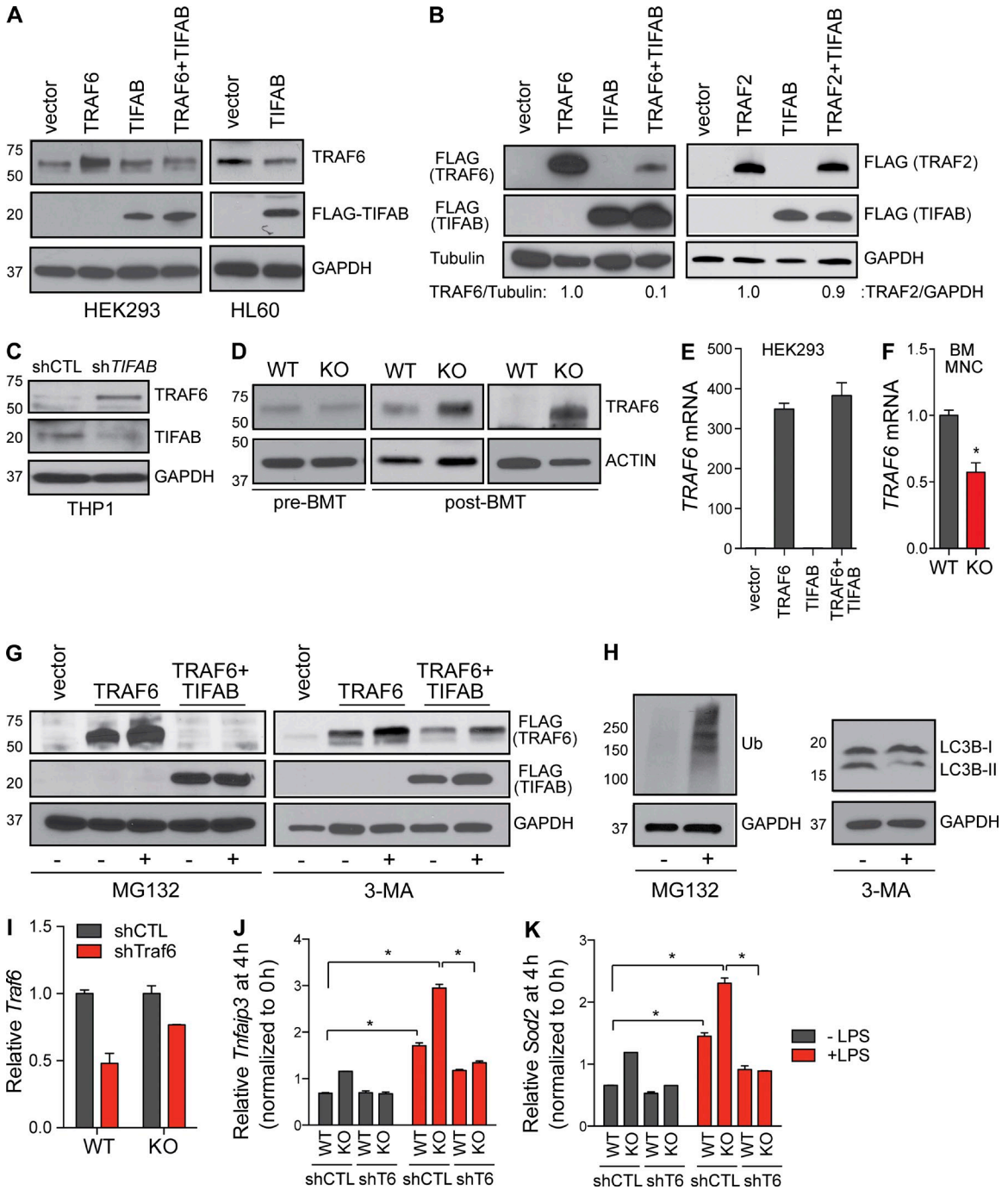

Figure 6. TIFAB inhibits TLR4 signaling by inducing degradation of TRAF6 protein via lysosomes. (A) Immunoblot analysis of HEK293 cells transfected with empty vector, TRAF6, or FLAG-TIFAB (left), and HL60 cells transduced with empty vector (pMSCV-pGK-GFP) or FLAG-TIFAB (right). Images are representative from at least three independent experiments. (B) Immunoblot analysis of HEK293 transfected with empty vector, TIFAB, and/or TRAF6 (left) or TRAF2 (right). Images are representative from at least two independent experiments. (C) Immunoblot analysis of human THP1 cells transduced with scrambled control shRNA (shCTL) or an shRNA targeting human TIFAB (sh*TIFAB*). (D) Immunoblot analysis for TRAF6 on *Tifab* WT or KO BM cells from independent pre and post-transplanted mice. (E) Expression analysis of TRAF6 mRNA by qRT-PCR in HEK293 cells transfected with empty vector, TRAF6, and/or FLAG-TIFAB. (F) Expression analysis of *Tifab* or *Traf6* mRNA by qRT-PCR in *Tifab* WT and KO BM cells. (G) Immunoblot analysis of HEK293 transfected with empty vector, TIFAB, and/or TRAF6, and then treated with a proteasome inhibitor (MG132, 10 µM for 12 h) or a lysosome inhibitor (3-MA, 5 mM for 24 h). Images are representative from at least three independent experiments. (H) HEK293 cells were treated with MG132 or 3-MA as in G, and immunoblotted for total ubiquitin (Ub) and LC3B, respectively. (I) Expression analysis of *Traf6* mRNA in *Tifab* WT or KO-transduced BM MNC expressing a scrambled control shRNA (shCTL) or an shRNA targeting mouse Traf6 (sh*Traf6*). (J and K) QRT-PCR expression analysis of *Tnfaip3* (J) and *Sod2* (K) in *Tifab* WT or KO BM MNC expressing a scrambled control shRNA (shCTL) or an shRNA-targeting mouse Traf6 (sh*Traf6*) after stimulation with LPS (100 ng/ml) for 4 h. Data are summarized from biological and technical replicates. Error bars are mean ± SEM values. *, $P < 0.05$; Student's *t* test.

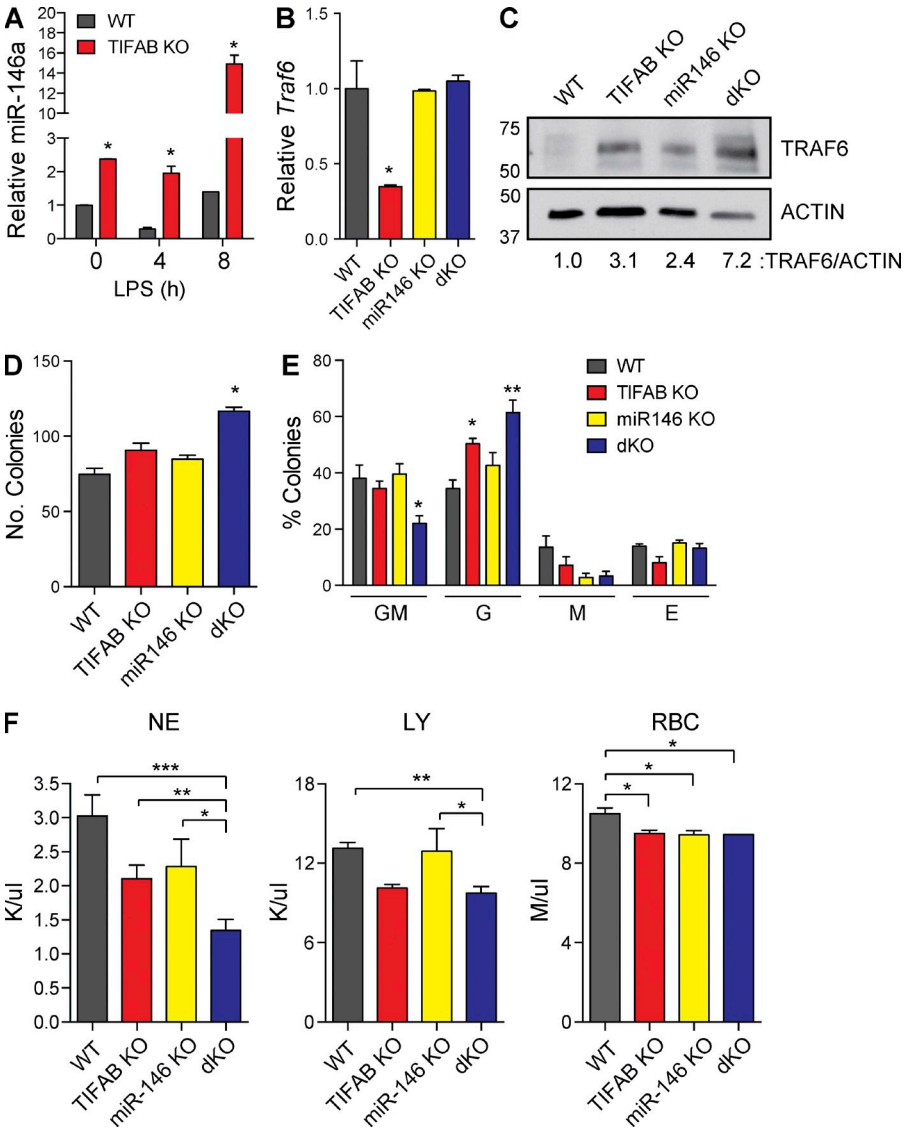

Figure 7. TIFAB and miR-146a cooperate to regulate TRAF6 and hematopoietic function. (A) Expression analysis of miR-146a in WT and KO BM MNC by qRT-PCR after stimulation with LPS (100 ng/ml) for the indicated time points. Expression was normalized to time 0 (1.0). *, $P < 0.05$; Student's *t* test. (B) Expression analysis of *Traf6* mRNA by qRT-PCR in WT, *Tifab* KO, miR-146a KO, and double KO (dKO) BM cells. *, $P < 0.05$; Student's *t* test. (C) Immunoblot analysis for TRAF6 on WT, *Tifab* KO, miR-146a KO, and dKO BM cells from transplanted mice. (D) Total colony-forming cells in methylcellulose from BM MNC from WT, *Tifab* KO, miR-146a KO, and dKO BM ($n = 5$–6; two independent experiments). *, $P < 0.05$; Student's *t* test. (E) Proportion of colonies formed from D. GM, granulocyte-monocyte; G, granulocyte; M, monocyte; E, erythroid (BFU-E). **, $P < 0.01$. (F) PB counts from mice transplanted with WT, *Tifab* KO, miR-146a KO, and dKO BM cells at 4 mo after transplant ($n > 8$ per group). Two independent transplantations experiments were performed. NE, neutrophils; LY, lymphocytes; and RBC, red blood cells. Error bars are mean ± SEM values. *, $P < 0.05$; **, $P < 0.01$; ***, $P < 0.001$, Student's *t* test.

Collectively, these findings suggest that two 5q genes, miR-146a and TIFAB, cooperate to regulate TRAF6 expression, whereas loss of both genes accentuates hematopoietic myeloid differentiation defects in vitro and in vivo.

Regulation of TRAF6 is dependent on the C-terminal domain of TIFAB

TIFAB is a 131 aa protein consisting of a conserved 55-aa forkhead-associated (FHA) domain (aa 36–91), whereas the residues flanking the FHA domain do not contain conserved motifs. To determine whether the FHA domain is required for regulating TRAF6 protein stability and signaling, we created deletion mutants of TIFAB. Three key mutants were created that removed the FHA domain (Δ35–91), the N-terminal domain (Δ1–34), or the C-terminal domain (Δ92–161). Additional TIFAB mutants were generated that deleted a combination of the aforementioned domains (Δ1–91 and Δ35–161; Fig. 8 A). The effects of TIFAB mutants on basal NF-κB activation were measured by κB-site reporter assays. Overexpression of TIFAB repressed basal κB-luciferase activation by ∼30% ($P = 0.01$; Fig. 8 B). Of the TIFAB deletion mutants, only Δ1–91 mutant retained its ability to repress κB-luciferase activation ($P = 1.7 \times 10^{-4}$; Fig. 8 B). We next evaluated the effects of the TIFAB mutants on TRAF6-mediated NF-κB activation. Overexpression of TRAF6 results in ∼40-fold increase in κB-luciferase activation (Fig. 8 C). Co-expression of full-length TIFAB resulted in >90-fold repression of TRAF6-mediated κB-luciferase activation ($P < 0.01$; Fig. 8 C). Surprisingly, deletion of the FHA domain (Δ35–91) still repressed TRAF6-mediated κB-luciferase activation and reduced TRAF6 protein levels (Fig. 8, C and D), suggesting that the FHA domain is not essential for inhibiting TRAF6-induced NF-κB signaling. Consistent with the effects on basal NF-κB activation, the Δ1–91 mutant also inhibited TRAF6-mediated NF-κB activation ($P = 0.002$; Fig. 8 C). To identify the essential residues within aa 92–161 of the Δ1–90 mutants that are

responsible for inhibiting TRAF6-mediated NF-κB activation, we created mutants that eliminated a portion of the C-terminal domain; Δ126–161 is missing the distal region of the C-terminal domain, and Δ91-126 is missing the proximal region of the C-terminal domain (Fig. 8 A). Both mutants retained their inhibitory effects on NF-κB, suggesting that multiple regions within this domain are essential for TIFAB function. In parallel, we also examined the effects of the TIFAB mutants on TRAF6 protein stability. Congruent with the NF-κB reporter assays, TIFAB mutant Δ1–91 suppressed TRAF6 protein nearly as efficiently as full-length TIFAB, strongly indicating that <70 aa within the C-terminal domain of TIFAB elicit TRAF6 degradation (Fig. 8, A and D).

Restoring TIFAB expression in MDS/AML cells induces apoptosis and impairs leukemic function

To establish the relevance of TIFAB in MDS and AML, TIFAB was reexpressed in three human MDS/AML cell lines (MDSL, HL60, and THP1) with low endogenous TIFAB, and assessed for leukemic progenitor function and survival. The level of TIFAB reexpression in the indicated cell lines was consistent with physiological TIFAB expression in primary normal and del(5q) AML BM MNC (Fig. 9 A). Ectopic expression of TIFAB in all three cell lines significantly reduced leukemic colony formation (Fig. 9 B) and survival (Fig. 9, C and D). To examine the cellular effects of restoring just the minimal TIFAB domain that retains TRAF6 inhibition in disease-relevant cells, we transduced the three MDS/AML cell lines with Δ1-91–expressing vectors. As a negative control, Δ92–161 was also expressed, as this mutant has lost its TRAF6/NF-κB inhibitory function, yet it still retains the FHA domain (Fig. 8 A). Restoring only the C-terminal domain (Δ1–91) suppressed MDS/AML leukemic progenitor function at a level comparable to WT TIFAB (Fig. 9 B). In stark contrast, Δ92–161 expression did not inhibit MDS/AML cell colony formation. Thus, restoring only the C-terminal domain of TIFAB is sufficient to destabilize TRAF6 protein, suppress NF-κB activation, and impair MDS/AML cell function.

To examine the effects of TIFAB reexpression on MDS/AML cell function in vivo, MDSL cells were transduced with TIFAB or empty vector (vector) and then xenografted into NSGS mice. Vector- and TIFAB-expressing MDSL cells

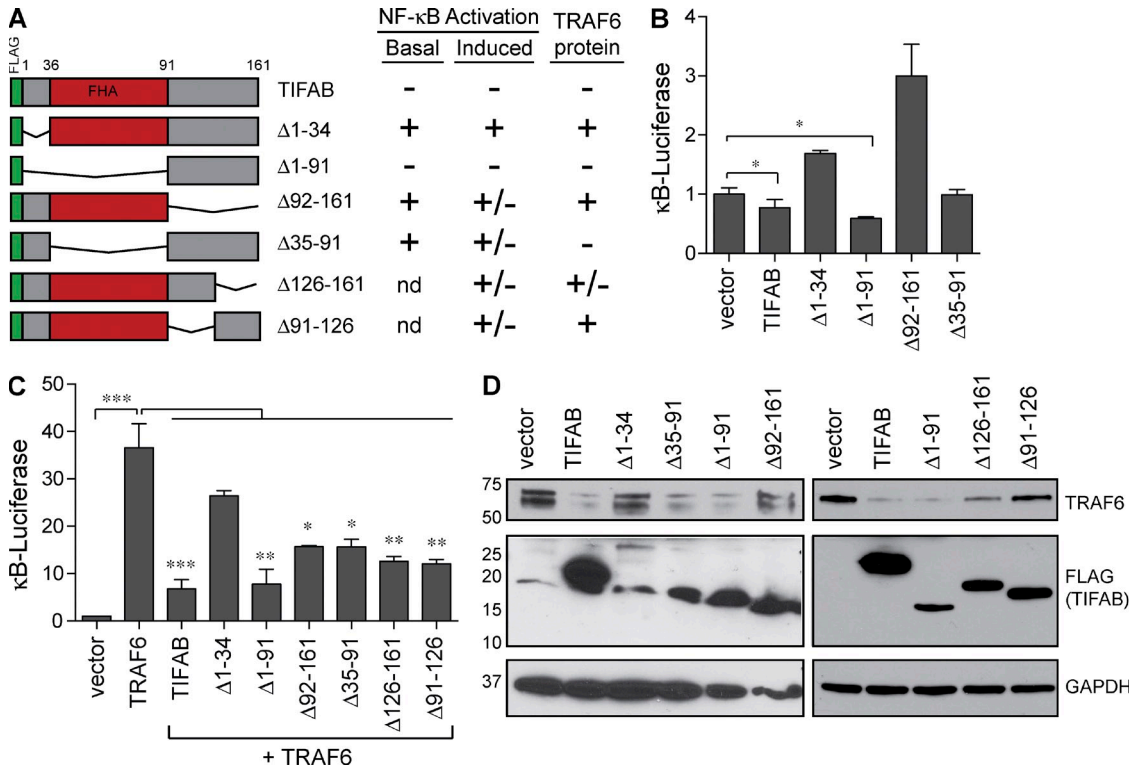

Figure 8. Inhibition of TRAF6 and NF-κB signaling depends on the TIFAB C-terminal domain and is independent of the FHA domain. (A) Overview of WT TIFAB and various TIFAB deletion mutants. Summary of NF-κB activation in HEK293 cells after expression of TIFAB mutants under basal (B) and TRAF6-induced conditions (C). Summary of TRAF6 protein expression in HEK293 cells after expression of TIFAB mutants (D). FHA, fork-head associated domain; FLAG, FLAG motif cloned at the N-terminal region of TIFAB mutants; nd, not determined. −, repression; +, normal levels; +/−, moderate repression. (B) NF-κB activation was measured by a κB-site containing reporter assays in HEK293 cells transfected with empty vector, TIFAB, or the indicated TIFAB deletion mutants. Values are normalized to Renilla-luciferase and empty vector (1.0). *, $P < 0.05$; Student's *t* test. (C) NF-κB activation was measured by κB-site containing reporter assays in HEK293 cells transfected with empty vector, TRAF6, and TIFAB or the indicated TIFAB deletion mutants. Values are normalized to Renilla-luciferase and empty vector (1.0). *, $P < 0.05$; **, $P < 0.01$; ***, $P < 0.001$; Student's *t* test. (D) Immunoblot analysis of HEK293 transfected with empty vector, TRAF6, and TIFAB or TIFAB deletion mutants. Error bars are mean ± SEM values.

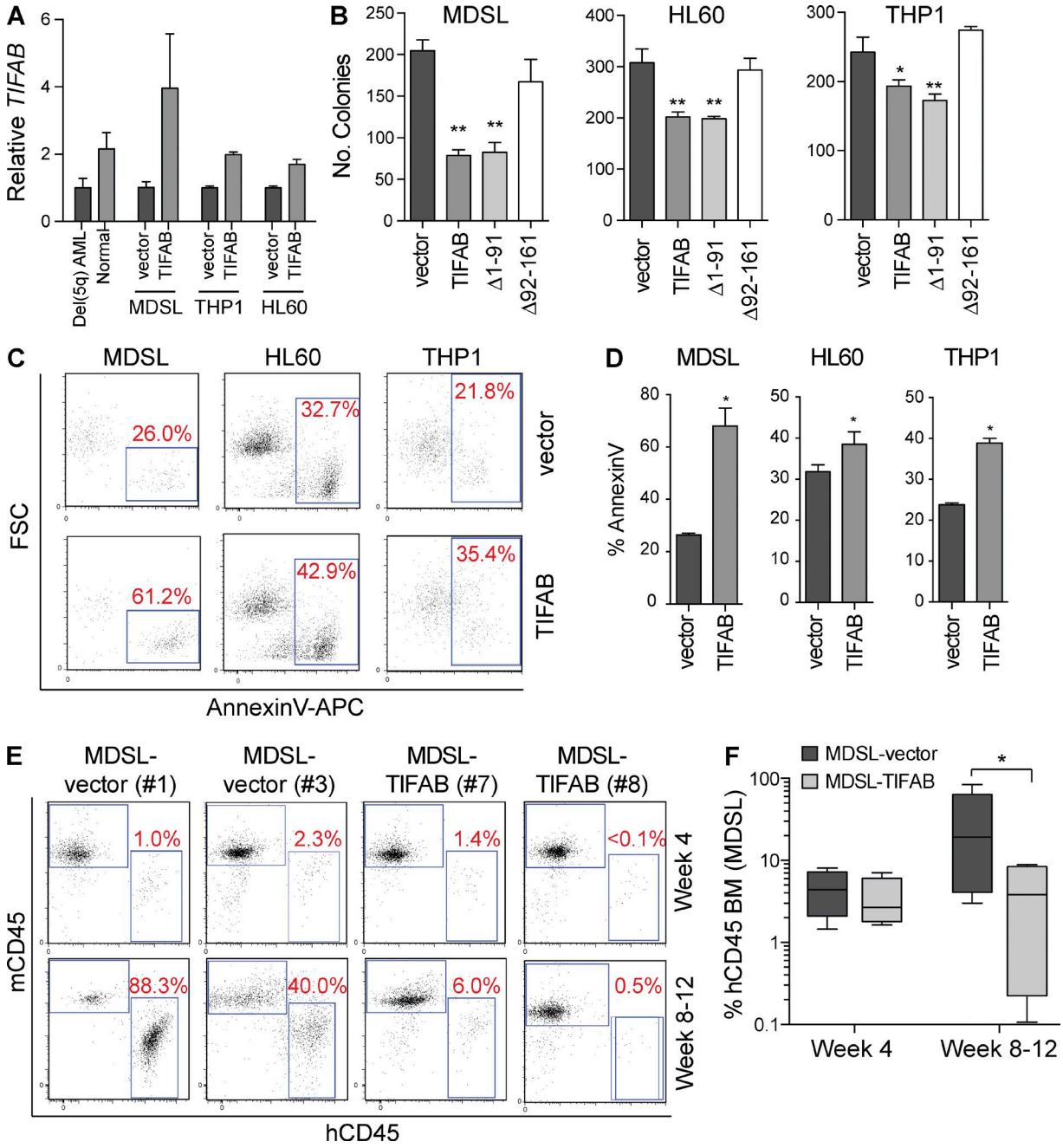

Figure 9. TIFAB reexpression suppresses MDS/AML cells. (A) Relative TIFAB mRNA expression determined by qRT-PCR from normal and del(5q) AML patient BM MNC, and transduced cell lines with empty vector or FLAG-TIFAB. (B) Colony formation in methylcellulose of MDSL, HL60, and THP1 cells transduced with empty vector, FLAG-TIFAB, FLAG-TIFABΔ1-91, FLAG-TIFABΔ92-161 was measured after 7–9 d. *, $P < 0.05$; **, $P < 0.01$; Student's *t* test. (C) Representative Annexin V staining for MDSL, HL60, and THP1 cells transduced with empty vector or FLAG-TIFAB (top). (D) The corresponding summary for Annexin V staining is shown for more than two independent experiments (bottom). *, $P < 0.05$; Student's *t* test. (E) MDSL cells transduced with vector or TIFAB were engrafted into NSGS mice ($n = 6$/group) and monitored for BM chimerism at the indicated time points. BM engraftment is shown for individual mice transplanted with vector (#1 and #3)-MDSL and TIFAB (#7 and #8)-MDSL cells at 4 and 8–12 wk (human versus mouse CD45). Percent of human cell (MDSL) engraftment is shown for the representative mice. (F) Summary of BM engraftment for mice transplanted with vector- and TIFAB-MDSL cells ($n > 5$ mice per group). *, $P < 0.05$; Student's *t* test.

efficiently engrafted into the BM of recipient mice within 4 wk (Fig. 9, E and F). However, beyond 8 wk after transplant, the BM engraftment of TIFAB-expressing MDSL cells dramatically diminished ($P = 0.04$), whereas control MDSL cells increased their engraftment during this time (Fig. 9, E and F). Thus, restoring TIFAB expression in MDS/AML cells induces apoptosis and impairs disease-propagating function in vitro and in vivo.

DISCUSSION

Identification and investigation of relevant del(5q) genes is vital to advancing our knowledge and treatment approach for del(5q) MDS/AML. Herein, we describe a TRAF6-interacting protein, TIFAB, which resides within the minimally deleted segment on 5q31.1. Hematopoietic-specific deletion of *Tifab* results in hematopoietic defects, including skewed HSPC proportions, altered myeloid differentiation, and cytopenia. A subset of mice transplanted with *Tifab*-deficient hematopoietic cells develop a BMF-like disease associated with BM dysplasia and cytopenia, which occurs through cell-intrinsic defects in HSPCs. Gene expression analysis of *Tifab*-deficient HSCs identified dysregulation of HSC- and immune-related gene signatures, and hypersensitivity to immune pathway stimulation downstream of TLR4. As therapeutic insight, re-expression of TIFAB results in an attenuated immune response and impaired del(5q) leukemic cell function.

Loss of TIFAB in HSPCs increases TRAF6 protein stability, which results in altered innate immune responsiveness and hematopoietic dysfunction. Evidence that TRAF6 is associated with MDS came from work related to miR-146a (Starczynowski et al., 2010, 2011). TRAF6 and IRAK1 are two key targets of miR-146a. In mouse HSPCs, overexpression of miR-146a results in reduced endogenous TRAF6 and IRAK1 protein, and conversely, knockdown of miR-146a results in derepression of TRAF6 and IRAK1 protein. Human miR-146a also resides on chr 5q and is deleted in ∼80% of del(5q) MDS and AML (Gondek et al., 2008). miR-146a$^{-/-}$ mice develop early onset myeloid expansion in the BM, and progress to more aggressive diseases such as lymphomas, BMF, and myeloid leukemia (Lu et al., 2010; Boldin et al., 2011; Zhao et al., 2011), in part due to derepression of TRAF6 and IRAK1. Given that TIFAB and miR-146a reside within the deleted region on chr 5q and are co-deleted in the majority of del(5q) MDS/AML patients, loss of TIFAB and miR-146a may cooperate to induce TRAF6 signaling. Deletion of miR-146a increases translation of TRAF6, whereas loss of TIFAB increases TRAF6 protein stability. Consistent with these previous observations, our combined deletion of TIFAB and miR-146a resulted in an additive increase in TRAF6 protein expression and subsequent innate immune signaling. Moreover, transplanted *Tifab*$^{-/-}$;miR-146a$^{-/-}$ BM cells exhibit worse cytopenias as compared with the individual gene knockout mice. In del(5q) MDS and AML, miR-146a deficiency also results in overexpression of a neighboring haploid gene, *SQSTM1* (p62), from the intact 5q allele to sustain TRAF6-mediated activation of NF-κB, and leukemic cell survival (Fang et al., 2014). This recent finding provides evidence that myeloid malignancies with del(5q) acquire a partial dependency on TRAF6 activation.

DIAPH1, which encodes mDia1, is located within the deleted segment on chr 5q and also regulates innate immune signaling. mDia1 belongs to the formin protein family and plays an important role in linear actin polymerization (Tominaga et al., 2000). *mDia1*-deficient cells express high levels of CD14, the co-receptor for the TLR4 and MD-2 complex, which detects LPS and damage-associated molecular pattern molecules (DAMP). *mDia1*-deficient mice exhibit an age-dependent granulocytopenia, and myeloid dysplasia, in part through increased TLR4 signaling. This underscores the connection between mDia1 and innate immune signaling in del(5q) MDS. Collectively, at least three verified haploinsufficient genes on chr 5q (miR-146a, *TIFAB*, and *DIAPH1*) regulate innate immune signaling and contribute to aspects of del(5q) MDS.

Mounting evidence also implicates increased innate immune signaling within HSPCs in the pathogenesis of nondel(5q) MDS. Chronic immune stimulation increases the risk for MDS and AML (Kristinsson et al., 2011). Overexpression of IL-1RAP and TLRs in MDS mediates the activation of TRAF6 and IRAK1 (Barreyro et al., 2012; Wei et al., 2012). Somatic activating mutation variants of TLR2 in MDS mediate hyperactivation of IRAK1 and NF-κB (Wei et al., 2012). Through noncell autonomous mechanisms, expansion of myeloid derived suppressor cells expressing S100A9 induces MDS in mice by activating TLR signaling (Chen et al., 2013). Lastly, the importance of TRAF6 in primary MDS is described in our recent publication, in which genetic and pharmacologic inhibition of IRAK1 suppresses TRAF6 activation and the MDS clone (Rhyasen et al., 2013a,b). Although NF-κB is one pathway activated by the innate immune complex, signaling networks regulated by TRAF6 in MDS and overt leukemia may be distinct, particularly as they relate to disease initiation versus maintenance. Further investigation into deciphering the importance of TRAF6-dependent NF-κB and non-NF-κB signaling networks during disease evolution and within distinct MDS/AML subtypes is warranted. Notably, constitutive NF-κB activation is not sufficient to induce MDS in mice (Beg et al., 1995; Rupec et al., 2005), suggesting additional pathways downstream of TRAF6 contribute to MDS initiation, whereas NF-κB may contribute to the maintenance of the disease (Breccia and Alimena, 2010).

TIFA was first identified as a TRAF6-interacting protein in a yeast two-hybrid screen (Kanamori et al., 2002; Takatsuna et al., 2003). TIFA interacts with TRAF6 through a consensus TRAF6-binding motif (Takatsuna et al., 2003) to promote TRAF6 oligomerization and subsequent activation of NF-κB (Ea et al., 2004). A mutation in TIFA that prevents binding to TRAF6 abolishes its ability to induce TRAF6 oligomerization and ubiquitination, indicating that this process requires direct interaction between TIFA and TRAF6 (Ea et al., 2004). TIFAB was identified as a TIFA-related protein by an in silico homology screen (Matsumura et al., 2004, 2009). Consistent with TIFA, we show by coimmunoprecipitation experiments that TIFAB and TRAF6 also form a complex in cells, and that this interaction primarily occurs in the cytoplasm. However, in contrast to the positive regulation of TIFA on TRAF6/NF-κB, herein we provide evidence that TIFAB is a negative regulator of innate immune signaling in HSPCs by inducing TRAF6 protein degradation through a lysosome-dependent mechanism. Regulation of TRAF proteins by autophagy/lysosomes has been previously described. Recently,

we have reported that proteosome inhibition induces autophagy/lysosome-dependent degradation of TRAF6 protein in MDS and AML cells (Fang et al., 2012). In this study, treatment with proteasome inhibitors reduced TRAF6 protein, which coincided with apoptosis of MDS/AML cells. TRAF6 is also degraded by autophagy in cells treated with double-stranded RNA, which can be blocked by addition of 3-MA (Inomata et al., 2012). Collectively, TRAF6 protein stability is controlled by lysosome-mediated degradation, in part through a TIFAB-dependent mechanism.

Both TIFA and TIFAB contain a FHA domain, a phosphopeptide recognition motif associated with DNA damage, signal transduction, vesicular transport, and protein degradation (Mahajan et al., 2008). Interestingly, deletion of the TIFAB FHA domain was not sufficient to prevent TIFAB-mediated degradation of TRAF6 or inhibition of NF-κB signaling. Thus it is possible that TIFAB is involved in several molecular functions: some that depend on its FHA domain, whereas others do not. In addition to changes in immune-related gene signatures, dysregulation of p53 gene signatures was also observed in *Tifab*$^{-/-}$ HSPCs. TIFAB may regulate both p53- and immune-related pathways as the TIFAB-deficient phenotype occurs primarily after hematopoietic stress. In conclusion, TIFAB is not only associated in the pathogenesis of del(5q) MDS/AML but also in regulating TLR-mediated signaling during inflammation.

MATERIALS AND METHODS

Knockout mice. A target vector was designed to replace exon 3, which contains all coding region of *Tifab*, with a β-galactosidase-loxP-neomycin resistant gene cassette-loxP fragment. Diphtheria toxin A gene cassette was inserted at the downstream end of the short arm. The targeting construct was electroporated into a 129-derived embryonic stem (ES) cell line. G418-resistant ES clones were screened for homologous recombination by Southern blot analysis. ES clones containing the correctly targeted *Tifab* locus were injected into C57BL/6 blastocysts. Male chimeric mice were mated with C57BL/6 J, and agouti pups carrying the correct target locus were used as F1 mice. F1 mice were crossed with transgenic mice expressing CRE under control of CAG promoter (Sakai and Miyazaki, 1997). Pups lacking neomycin-resistant gene cassette were further backcrossed into the C57BL/6 J background. miR-146a$^{-/-}$ C57BL/6 mice were obtained from D. Baltimore (California Institute of Technology, Pasadena, CA) as previously described (Fang et al., 2014). Animals were bred and housed in the Association for Assessment and Accreditation of Laboratory Animal Care-accredited animal facility of Cincinnati Children's Hospital Medical Center.

Bone marrow transplantation. For noncompetitive BM transplantation, BM mononuclear cells (0.3–3 × 10^6) from C7BL/6 *Tifab*$^{+/+}$, *Tifab*$^{+/-}$, *Tifab*$^{-/-}$, miR-146a$^{-/-}$, or *Tifab*$^{-/-}$;miR-146a$^{-/-}$ mice were injected i.v. into lethally radiated (7.0 Gy and 4.75 Gy after 3 h) syngeneic recipient Boy/J mice. For competitive BM transplants, BM mononuclear cells (3 × 10^5) from 8-wk-old CD45.2 *Tifab*$^{+/+}$, *Tifab*$^{+/-}$, or *Tifab*$^{-/-}$ mice were mixed with equal numbers of 8-wk-old BM mononuclear cells from BoyJ (CD45.1) mice and then injected i.v. into lethally irradiated (7.0 Gy and 4.75 Gy after 3 h) CD45.1 recipient BoyJ mice.

BM and PB analysis. For cytospins, 2.5–5 × 10^5 BM cells were spun onto slide at 300 rpm for 5 min, and then stained with Wright-Giemsa. For BM sections, tibia were fixed in formalin and then stained with hematoxylin and eosin. Complete blood counts were performed on PB isolated from the tail vein every 4 wk and analyzed using the Drew Scientific Hemavet 950.

BM stimulation with LPS and TNF. BM mononuclear cells were harvested from *Tifab*$^{+/+}$ and *Tifab*$^{-/-}$ mice and cultured in the presence of vehicle control (dH_2O for LPS or 0.1% BSA in 1X PBS for TNF), ultrapure LPS (100 ng/ml; Invitrogen), or TNF (10 ng/ml; Gibco) for 0, 1, 4, and 8 h. RNA extraction, cDNA conversion, and qRT-PCR analysis were performed as described below.

Quantitative PCR analysis. RNA was extracted from cells and purified with TRIzol Reagent (Life Technologies) or Quick-RNA MiniPrep kit (Zymo Research). cDNA was generated using a high capacity RNA to cDNA kit (Life Technologies 4387406 or 4368814). qPCR was performed using TaqMan Master mix and the following probes (Life Technologies): *TIFAB* (Hs04185733_m1), *Tifab* (Mm0421026_m1), *TRAF6* (Hs00371512_g1), *Traf6* (Mm00493836_m1), *Il6* (Mm00446190_m1), *Bcl2a1* (Mm03646861_mH), *Tnfaip3* (Mm00437121_m1), *Sod2* (Mm01313000_m1), *GAPDH* (Hs02758991_g1), and *Gapdh* (Mm99999915_g1). qPCR was performed on an Applied Biosystems StepOne Plus Real-Time PCR System. miR-146a expression was performed as previously described (Starczynowski et al., 2011).

Clonogenic progenitor assays. Hematopoietic clonogenic progenitor frequencies were determined by plating 2 × 10^5 BM cells/ml isolated from *Tifab*$^{+/+}$, *Tifab*$^{+/-}$, *Tifab*$^{-/-}$, miR-146a$^{-/-}$, or *Tifab*$^{-/-}$;miR-146a$^{-/-}$ mice in methylcellulose media containing human erythropoietin, murine SCF, murine IL-3, and human IL-6 (Methocult M3434; Stem Cell Technologies). For human leukemic colony formation, transduced MDSL, HL-60, and THP1 cells were plated at 2–3 × 10^4/ml in methylcellulose (Methocult H4434; Stem Cell Technologies). Colonies were scored after 10 d.

Cell lines. Human AML cell lines HL60 and THP1 were purchased from ATCC. The myelodysplastic cell line, MDSL, was provided by K. Tohyama (Kawasaki Medical School, Okayama, Japan). HEK293 cells were also purchased from ATCC. HL-60 and THP1 cell lines were cultured in RPMI-1640 medium with 10% FBS and 1% penicillin-streptomycin. HEK293 cells were cultured in DMEM with 10% FBS and 1% penicillin-streptomycin. MDSL were cultured in 10% FBS, 1% penicillin-streptomycin, 20 ng/ml IL-3, and 50 μM β-mercaptoethanol. Human marrow-derived mononuclear cells were obtained from the Translational Research Development Support Laboratory of Cincinnati Children's Hospital (Cincinnati, OH) under an approved Institutional Review Board protocol. Trypan blue exclusion was performed to determined cell proliferation and viability.

Gene expression profiling. Gene expression analysis (MoGene 2.0 ST Array) was performed on sorted LSK isolated from 3-mo-old mice transplanted with *Tifab*$^{+/+}$ or *Tifab*$^{-/-}$ BM cells (n = 3 mice/group). Total RNA was extracted and purified with Quick RNA extraction kit (Zymo Research). Total RNA was reverse transcribed, labeled, and hybridized onto the GeneChip MoGene 2.0 ST Array (Affymetrix). Scanning was performed with GeneChip Version 3.2 Scanner 3000 7G (Affymetrix) and evaluated with GeneChip operating software (Affymetrix). Data analysis was performed using GeneSpring GX 11.5 software (Agilent Technologies). Gene set enrichment analysis was performed on a JAVA-based dataset supported by the Broad Institute (Subramanian et al., 2005).

Flow cytometry analysis. Antibodies used for flow cytometric analysis of BM and PB cells are listed in Table S2). All FACS analyses were performed on FACSAria or FACSCanto machines (BD). FACS data analysis was performed using FACSDiva (BD) or FlowJo (Tree Star) software.

Immunoprecipitation and immunoblotting. Total protein was isolated from cells by lysing samples in RIPA buffer (50 mM Tris-HCl, 150 mM NaCl, 1 mM EDTA, 1% Triton X-100, and 0.1% SDS), in the presence of PMSF, sodium orthovanadate, and protease and phosphatase inhibitors. For immunoprecipitation, TRAF6 or hemagglutinin (HA) antibodies were added to cell lysates for 2 h at 4°C and captured by the addition of Protein A/G Plus beads (sc-2003; Santa Cruz Biotechnology, Inc.). The immune

complexes were washed with RIPA lysis buffer, and resuspended in SDS sample buffer. Proteins were separated by SDS-PAGE, transferred to nitrocellulose membranes, and analyzed by immunoblotting. Immunoblotting was performed with the following antibodies: TRAF6 (sc-7221; Santa Cruz Biotechnology, Inc.), FLAG (F3165; Sigma-Aldrich), HA (H6908; Sigma-Aldrich) GAPDH (5174; Cell Signaling Technology), phospho-IKKβ (2697; Cell Signaling Technology), IKKβ (2370; Cell Signaling Technology), and Actin (4968; Cell Signaling Technology).

Plasmids and transfection. WT and mutant TIFAB cDNA were created by custom gene synthesis (IDT). FLAG and/or HA tags were inserted in frame at the 5′-end of human TIFAB. FLAG-TIFAB was cloned into pcDNA3.0 with EcoRI and HindIII, and into pMSCV-pGK-GFP with EcoRI and XhoI. pcDNA3.0-FLAG-IKKβ and pcDNA3.0-FLAG-RelA were purchased from Addgene. pcDNA3.0-FLAG-TRAF2 was a gift from H. Habelhah (University of Iowa, Iowa City, IA). pcDNA3.0-FLAG-TRAF6 was created by subcloning TRAF6 from MIY-TRAF6 using EcoRI. FLAG-TRAF6 was cloned into pMSCV-pGK-GFP with EcoRI and XhoI. Transfections were performed using TransIT-LT1 transfection reagent (Mirus MIR 2306). HEK293 cells were transfected for 24–48 h with κB-luciferase and TK Renilla plasmids along with TRAF6, TIFAB, TRAF2, IKKβ, or p65. Lysates were analyzed for NF-κB reporter activity using the dual luciferase reporter assay system (Promega E1910). Retro- and lentiviral transduction of cells has been previous described (Fang et al., 2014). For HL60 and THP1, cells were transduced with virus encoding vectors coexpressing GFP (pMSCV-pGK-GFP or pLeGo-iG2). GFP-positive cells were FACS sorted using a FACSAria (BD). For knockdown of *Traf6* in *Tifab*$^{+/+}$ or *Tifab*$^{-/-}$ BM mononuclear cells, BM cells were isolated and transduced with pLKO.1 lentiviral vectors (OpenBiosystems) encoding shRNAs targeting mouse Traf6 (TRCN0000040735), as previously described (Fang et al., 2014).

Purification and mass spectrometry analysis of TIFAB-interacting proteins. TIFAB complexes were isolated from cytosolic and nuclear extracts of HL60 cells transduced with HA/FLAG-TIFAB using a two-step affinity purification procedure. TIFAB-interacting proteins were identified by mass spectrometry analysis, using a previously described procedure (Singh et al., 2008).

Xenograftment of NSGS with MDSL cells. MDSL cells were transduced to overexpress TIFAB (pGK-TIFAB-GFP), and GFP-positive cells were isolated by flow cytometry. 1×10^6 MDSL cells were intravenously injected into 8-wk old-conditioned (Busulfan) NOD/SCID-IL2Rγ3GS (NSGS) mice as previously described (Rhyasen et al., 2013a, 2014). BM aspirates were performed to measure MDSL engraftment by flow cytometry (human CD45.1 versus mouse CD45.1).

Microarray data. Microarray data can be found in the Gene Expression Omnibus database under accession no. GSE72936.

Patient samples. Informed consent was obtained according to protocols approved by the review board of Cleveland Clinic. Diagnoses were reviewed at Cleveland Clinic and adapted, when required, to WHO 2008 criteria. For qRT-PCR analysis of *TIFAB* transcript, BM mononuclear cells were isolated from MDS/AML patients and age-matched healthy controls, as previously described (Fang et al., 2014).

Online supplemental material. Table S1 lists genes differentially expressed in Tifab-deficient LSK by >1.7 fold. Table S2 lists antibodies for flow cytometry. Online supplemental material is available at http://www.jem.org/cgi/content/full/jem.20141898/DC1.

We thank Jeff Bailey and Victoria Summey for assistance with transplantations (Comprehensive Mouse and Cancer Core). We also thank Shawn Smith for his assistance with the gene expression profiling (Microarray Core).

This work was supported by Cincinnati Children's Hospital Research Foundation, American Society of Hematology (ASH), National Institutes of Health (RO1HL111103), Gabrielle's Angel Foundation, and Department of Defense grants to DTS. JI was supported by grants-in-aid for Scientific Research on Innovative Areas from the Ministry of Education, Culture, Sports, Science, and Technology of Japan. AK was supported by a Canadian Institute of Health Research grant (MOP 133455). MV was supported by a T32 training grant from the National Institutes of Health (5T32ES007250-25).

The authors declare no competing financial interests.

Submitted: 3 October 2014
Accepted: 4 September 2015

REFERENCES

Barlow, J.L., L.F. Drynan, D.R. Hewett, L.R. Holmes, S. Lorenzo-Abalde, A.L. Lane, H.E. Jolin, R. Pannell, A.J. Middleton, S.H. Wong, et al. 2010. A p53-dependent mechanism underlies macrocytic anemia in a mouse model of human 5q- syndrome. *Nat. Med.* 16:59–66. http://dx.doi.org/10.1038/nm.2063

Barreyro, L., B. Will, B. Bartholdy, L. Zhou, T.I. Todorova, R.F. Stanley, S. Ben-Neriah, C. Montagna, S. Parekh, A. Pellagatti, et al. 2012. Overexpression of IL-1 receptor accessory protein in stem and progenitor cells and outcome correlation in AML and MDS. *Blood.* 120:1290–1298. http://dx.doi.org/10.1182/blood-2012-01-404699

Beg, A.A., W.C. Sha, R.T. Bronson, and D. Baltimore. 1995. Constitutive NF-kappa B activation, enhanced granulopoiesis, and neonatal lethality in I kappa B alpha-deficient mice. *Genes Dev.* 9:2736–2746. http://dx.doi.org/10.1101/gad.9.22.2736

Boldin, M.P., K.D. Taganov, D.S. Rao, L. Yang, J.L. Zhao, M. Kalwani, Y. Garcia-Flores, M. Luong, A. Devrekanli, J. Xu, et al. 2011. miR-146a is a significant brake on autoimmunity, myeloproliferation, and cancer in mice. *J. Exp. Med.* 208:1189–1201. http://dx.doi.org/10.1084/jem.20101823

Boultwood, J., C. Fidler, S. Lewis, S. Kelly, H. Sheridan, T.J. Littlewood, V.J. Buckle, and J.S. Wainscoat. 1994. Molecular mapping of uncharacteristically small 5q deletions in two patients with the 5q- syndrome: delineation of the critical region on 5q and identification of a 5q- breakpoint. *Genomics.* 19:425–432. http://dx.doi.org/10.1006/geno.1994.1090

Boultwood, J., C. Fidler, P. Soularue, A.J. Strickson, M. Kostrzewa, R.J. Jaju, F.E. Cotter, N. Fairweather, A.P. Monaco, U. Müller, et al. 1997. Novel genes mapping to the critical region of the 5q- syndrome. *Genomics.* 45:88–96. http://dx.doi.org/10.1006/geno.1997.4899

Boultwood, J., C. Fidler, A.J. Strickson, F. Watkins, M. Kostrzewa, R.J. Jaju, U. Müller, and J.S. Wainscoat. 2000. Transcription mapping of the 5q- syndrome critical region: cloning of two novel genes and sequencing, expression, and mapping of a further six novel cDNAs. *Genomics.* 66:26–34. http://dx.doi.org/10.1006/geno.2000.6193

Boultwood, J., C. Fidler, A.J. Strickson, F. Watkins, S. Gama, L. Kearney, S. Tosi, A. Kasprzyk, J.F. Cheng, R.J. Jaju, and J.S. Wainscoat. 2002. Narrowing and genomic annotation of the commonly deleted region of the 5q- syndrome. *Blood.* 99:4638–4641. http://dx.doi.org/10.1182/blood.V99.12.4638

Boultwood, J., A. Pellagatti, H. Cattan, C.H. Lawrie, A. Giagounidis, L. Malcovati, M.G. Della Porta, M. Jädersten, S. Killick, C. Fidler, et al. 2007. Gene expression profiling of CD34+ cells in patients with the 5q- syndrome. *Br. J. Haematol.* 139:578–589. http://dx.doi.org/10.1111/j.1365-2141.2007.06833.x

Breccia, M., and G. Alimena. 2010. NF-κB as a potential therapeutic target in myelodysplastic syndromes and acute myeloid leukemia. *Expert Opin. Ther. Targets.* 14:1157–1176. http://dx.doi.org/10.1517/14728222.2010.522570

Cazzola, M., and L. Malcovati. 2010. Prognostic classification and risk assessment in myelodysplastic syndromes. *Hematol. Oncol. Clin. North Am.* 24:459–468. http://dx.doi.org/10.1016/j.hoc.2010.02.005

Chen, X., E.A. Eksioglu, J. Zhou, L. Zhang, J. Djeu, N. Fortenbery, P. Epling-Burnette, S. Van Bijnen, H. Dolstra, J. Cannon, et al. 2013. Induction of myelodysplasia by myeloid-derived suppressor cells. *J. Clin. Invest.* 123:4595–4611. http://dx.doi.org/10.1172/JCI67580

Ea, C.K., L. Sun, J. Inoue, and Z.J. Chen. 2004. TIFA activates IkappaB kinase (IKK) by promoting oligomerization and ubiquitination of TRAF6. *Proc. Natl. Acad. Sci. USA*. 101:15318–15323. http://dx.doi.org/10.1073/pnas.0404132101

Ebert, B.L., J. Pretz, J. Bosco, C.Y. Chang, P. Tamayo, N. Galili, A. Raza, D.E. Root, E. Attar, S.R. Ellis, and T.R. Golub. 2008. Identification of RPS14 as a 5q- syndrome gene by RNA interference screen. *Nature*. 451:335–339. http://dx.doi.org/10.1038/nature06494

Fang, J., G. Rhyasen, L. Bolanos, C. Rasch, M. Varney, M. Wunderlich, S. Goyama, G. Jansen, J. Cloos, C. Rigolino, et al. 2012. Cytotoxic effects of bortezomib in myelodysplastic syndrome/acute myeloid leukemia depend on autophagy-mediated lysosomal degradation of TRAF6 and repression of PSMA1. *Blood*. 120:858–867. http://dx.doi.org/10.1182/blood-2012-02-407999

Fang, J., B. Barker, L. Bolanos, X. Liu, A. Jerez, H. Makishima, S. Christie, X. Chen, D.S. Rao, H.L. Grimes, et al. 2014. Myeloid malignancies with chromosome 5q deletions acquire a dependency on an intrachromosomal NF-κB gene network. *Cell Reports*. 8:1328–1338. http://dx.doi.org/10.1016/j.celrep.2014.07.062

Giagounidis, A.A., U. Germing, and C. Aul. 2006. Biological and prognostic significance of chromosome 5q deletions in myeloid malignancies. *Clin. Cancer Res*. 12:5–10. http://dx.doi.org/10.1158/1078-0432.CCR-05-1437

Gondek, L.P., R. Tiu, C.L. O'Keefe, M.A. Sekeres, K.S. Theil, and J.P. Maciejewski. 2008. Chromosomal lesions and uniparental disomy detected by SNP arrays in MDS, MDS/MPD, and MDS-derived AML. *Blood*. 111:1534–1542. http://dx.doi.org/10.1182/blood-2007-05-092304

Haase, D. 2008. Cytogenetic features in myelodysplastic syndromes. *Ann. Hematol*. 87:515–526. http://dx.doi.org/10.1007/s00277-008-0483-y

Haase, D., U. Germing, J. Schanz, M. Pfeilstöcker, T. Nösslinger, B. Hildebrandt, A. Kundgen, M. Lübbert, R. Kunzmann, A.A. Giagounidis, et al. 2007. New insights into the prognostic impact of the karyotype in MDS and correlation with subtypes: evidence from a core dataset of 2124 patients. *Blood*. 110:4385–4395. http://dx.doi.org/10.1182/blood-2007-03-082404

Inomata, M., S. Niida, K.I. Shibata, and T. Into. 2012. Regulation of Toll-like receptor signaling by NDP52-mediated selective autophagy is normally inactivated by A20. *Cell. Mol. Life Sci*. 69:963–979. http://dx.doi.org/10.1007/s00018-011-0819-y

Jaju, R.J., J. Boultwood, F.J. Oliver, M. Kostrzewa, C. Fidler, N. Parker, J.D. McPherson, S.W. Morris, U. Müller, J.S. Wainscoat, and L. Kearney. 1998. Molecular cytogenetic delineation of the critical deleted region in the 5q- syndrome. *Genes Chromosomes Cancer*. 22:251–256. http://dx.doi.org/10.1002/(SICI)1098-2264(199807)22:3<251::AID-GCC11>3.0.CO;2-R

Joslin, J.M., A.A. Fernald, T.R. Tennant, E.M. Davis, S.C. Kogan, J. Anastasi, J.D. Crispino, and M.M. Le Beau. 2007. Haploinsufficiency of EGR1, a candidate gene in the del(5q), leads to the development of myeloid disorders. *Blood*. 110:719–726. http://dx.doi.org/10.1182/blood-2007-01-068809

Kanamori, M., H. Suzuki, R. Saito, M. Muramatsu, and Y. Hayashizaki. 2002. T2BP, a novel TRAF2 binding protein, can activate NF-kappaB and AP-1 without TNF stimulation. *Biochem. Biophys. Res. Commun*. 290:1108–1113. http://dx.doi.org/10.1006/bbrc.2001.6315

Kristinsson, S.Y., M. Björkholm, M. Hultcrantz, A.R. Derolf, O. Landgren, and L.R. Goldin. 2011. Chronic immune stimulation might act as a trigger for the development of acute myeloid leukemia or myelodysplastic syndromes. *J. Clin. Oncol*. 29:2897–2903. http://dx.doi.org/10.1200/JCO.2011.34.8540

Kumar, M., A. Narla, A. Nonami, B. Ball, C. Chin, C. Chen, J.L. Kutok, N. Galili, A. Raza, E. Attar, et al. 2009. Coordinate Loss of a MicroRNA Mir 145 and a Protein-Coding Gene RPS14 Cooperate in the Pathogenesis of 5q- Syndrome. In American Society of Hematology, New Orleans, LA.

Le Beau, M.M., R.S. Lemons, R. Espinosa III, R.A. Larson, N. Arai, and J.D. Rowley. 1989. Interleukin-4 and interleukin-5 map to human chromosome 5 in a region encoding growth factors and receptors and are deleted in myeloid leukemias with a del(5q). *Blood*. 73:647–650.

Le Beau, M.M., R. Espinosa III, W.L. Neuman, W. Stock, D. Roulston, R.A. Larson, M. Keinanen, and C.A. Westbrook. 1993. Cytogenetic and molecular delineation of the smallest commonly deleted region of chromosome 5 in malignant myeloid diseases. *Proc. Natl. Acad. Sci. USA*. 90:5484–5488. http://dx.doi.org/10.1073/pnas.90.12.5484

Liu, T.X., M.W. Becker, J. Jelinek, W.S. Wu, M. Deng, N. Mikhalkevich, K. Hsu, C.D. Bloomfield, R.M. Stone, D.J. DeAngelo, et al. 2007. Chromosome 5q deletion and epigenetic suppression of the gene encoding alpha-catenin (CTNNA1) in myeloid cell transformation. *Nat. Med*. 13:78–83. http://dx.doi.org/10.1038/nm1512

Lu, L.F., M.P. Boldin, A. Chaudhry, L.L. Lin, K.D. Taganov, T. Hanada, A. Yoshimura, D. Baltimore, and A.Y. Rudensky. 2010. Function of miR-146a in controlling Treg cell-mediated regulation of Th1 responses. *Cell*. 142:914–929. http://dx.doi.org/10.1016/j.cell.2010.08.012

Mahajan, A., C. Yuan, H. Lee, E.S. Chen, P.Y. Wu, and M.D. Tsai. 2008. Structure and function of the phosphothreonine-specific FHA domain. *Sci. Signal*. 1:re12. http://dx.doi.org/10.1126/scisignal.151re12

Matsumura, T., K. Semba, S. Azuma, S. Ikawa, J. Gohda, T. Akiyama, and J. Inoue. 2004. TIFAB inhibits TIFA, TRAF-interacting protein with a forkhead-associated domain. *Biochem. Biophys. Res. Commun*. 317:230–234. http://dx.doi.org/10.1016/j.bbrc.2004.03.030

Matsumura, T., J. Kawamura-Tsuzuku, T. Yamamoto, K. Semba, and J. Inoue. 2009. TRAF-interacting protein with a forkhead-associated domain B (TIFAB) is a negative regulator of the TRAF6-induced cellular functions. *J. Biochem*. 146:375–381. http://dx.doi.org/10.1093/jb/mvp080

Pellagatti, A., M. Cazzola, A.A. Giagounidis, L. Malcovati, M.G. Porta, S. Killick, L.J. Campbell, L. Wang, C.F. Langford, C. Fidler, et al. 2006. Gene expression profiles of $CD34^+$ cells in myelodysplastic syndromes: involvement of interferon-stimulated genes and correlation to FAB subtype and karyotype. *Blood*. 108:337–345. http://dx.doi.org/10.1182/blood-2005-12-4769

Qian, Z., J.M. Joslin, T.R. Tennant, S.C. Reshmi, D.J. Young, A. Stoddart, R.A. Larson, and M.M. Le Beau. 2010. Cytogenetic and genetic pathways in therapy-related acute myeloid leukemia. *Chem. Biol. Interact*. 184:50–57. http://dx.doi.org/10.1016/j.cbi.2009.11.025

Rhyasen, G.W., L. Bolanos, J. Fang, A. Jerez, M. Wunderlich, C. Rigolino, L. Mathews, M. Ferrer, N. Southall, R. Guha, et al. 2013a. Targeting IRAK1 as a therapeutic approach for myelodysplastic syndrome. *Cancer Cell*. 24:90–104. http://dx.doi.org/10.1016/j.ccr.2013.05.006

Rhyasen, G.W., L. Bolanos, and D.T. Starczynowski. 2013b. Differential IRAK signaling in hematologic malignancies. *Exp. Hematol*. 41:1005–1007. http://dx.doi.org/10.1016/j.exphem.2013.09.008

Rhyasen, G.W., M. Wunderlich, K. Tohyama, G. Garcia-Manero, J.C. Mulloy, and D.T. Starczynowski. 2014. An MDS xenograft model utilizing a patient-derived cell line. *Leukemia*. 28:1142–1145. http://dx.doi.org/10.1038/leu.2013.372

Rupec, R.A., F. Jundt, B. Rebholz, B. Eckelt, G. Weindl, T. Herzinger, M.J. Flaig, S. Moosmann, G. Plewig, B. Dörken, et al. 2005. Stroma-mediated dysregulation of myelopoiesis in mice lacking I kappa B alpha. *Immunity*. 22:479–491. http://dx.doi.org/10.1016/j.immuni.2005.02.009

Sakai, K., and J. Miyazaki. 1997. A transgenic mouse line that retains Cre recombinase activity in mature oocytes irrespective of the cre transgene transmission. *Biochem. Biophys. Res. Commun*. 237:318–324. http://dx.doi.org/10.1006/bbrc.1997.7111

Schneider, R.K., V. Ademà, D. Heckl, M. Järås, M. Mallo, A.M. Lord, L.P. Chu, M.E. McConkey, R. Kramann, A. Mullally, et al. 2014. Role of casein kinase 1A1 in the biology and targeted therapy of del(5q) MDS. *Cancer Cell*. 26:509–520. http://dx.doi.org/10.1016/j.ccr.2014.08.001

Singh, T.R., A.M. Ali, V. Busygina, S. Raynard, Q. Fan, C.H. Du, P.R. Andreassen, P. Sung, and A.R. Meetei. 2008. BLAP18/RMI2, a novel OB-fold-containing protein, is an essential component of the Bloom helicase-double Holliday junction dissolvasome. *Genes Dev*. 22:2856–2868. http://dx.doi.org/10.1101/gad.1725108

Starczynowski, D.T., F. Kuchenbauer, B. Argiropoulos, S. Sung, R. Morin, A. Muranyi, M. Hirst, D. Hogge, M. Marra, R.A. Wells, et al. 2010. Identification of miR-145 and miR-146a as mediators of the 5q- syndrome phenotype. *Nat. Med*. 16:49–58. http://dx.doi.org/10.1038/nm.2054

Starczynowski, D.T., F. Kuchenbauer, J. Wegrzyn, A. Rouhi, O. Petriv, C.L. Hansen, R.K. Humphries, and A. Karsan. 2011. MicroRNA-146a disrupts

hematopoietic differentiation and survival. *Exp. Hematol.* 39:167–178: e4. http://dx.doi.org/10.1016/j.exphem.2010.09.011

Subramanian, A., P. Tamayo, V.K. Mootha, S. Mukherjee, B.L. Ebert, M.A. Gillette, A. Paulovich, S.L. Pomeroy, T.R. Golub, E.S. Lander, and J.P. Mesirov. 2005. Gene set enrichment analysis: a knowledge-based approach for interpreting genome-wide expression profiles. *Proc. Natl. Acad. Sci. USA.* 102:15545–15550. http://dx.doi.org/10.1073/pnas.0506580102

Takatsuna, H., H. Kato, J. Gohda, T. Akiyama, A. Moriya, Y. Okamoto, Y. Yamagata, M. Otsuka, K. Umezawa, K. Semba, and J. Inoue. 2003. Identification of TIFA as an adapter protein that links tumor necrosis factor receptor-associated factor 6 (TRAF6) to interleukin-1 (IL-1) receptor-associated kinase-1 (IRAK-1) in IL-1 receptor signaling. *J. Biol. Chem.* 278:12144–12150. http://dx.doi.org/10.1074/jbc.M300720200

Tominaga, T., E. Sahai, P. Chardin, F. McCormick, S.A. Courtneidge, and A.S. Alberts. 2000. Diaphanous-related formins bridge Rho GTPase and Src tyrosine kinase signaling. *Mol. Cell.* 5:13–25. http://dx.doi.org/10.1016/S1097-2765(00)80399-8

Wei, Y., R. Chen, S. Dimicoli, C.E. Bueso-Ramos, D.S. Neuberg, S.A. Pierce, H. Yang, Y. Jia, H. Zheng, Z. Fang, et al. 2012. Deregulation of TLR2-JMJD3 Innate Immunity Signaling, Including a Rare TLR2 SNP As a Potential Somatic Mutation. In Myelodysplastic Syndromes (MDS). In American Society of Hematology, Atlanta, GA.

Willman, C.L., C.E. Sever, M.G. Pallavicini, H. Harada, N. Tanaka, M.L. Slovak, H. Yamamoto, K. Harada, T.C. Meeker, A.F. List, et al. 1993. Deletion of IRF-1, mapping to chromosome 5q31.1, in human leukemia and preleukemic myelodysplasia. *Science.* 259:968–971. http://dx.doi.org/10.1126/science.8438156

Wu, H., and J.R. Arron. 2003. TRAF6, a molecular bridge spanning adaptive immunity, innate immunity and osteoimmunology. *BioEssays.* 25:1096–1105. http://dx.doi.org/10.1002/bies.10352

Zhao, N., A. Stoffel, P.W. Wang, J.D. Eisenbart, R. Espinosa III, R.A. Larson, and M.M. Le Beau. 1997. Molecular delineation of the smallest commonly deleted region of chromosome 5 in malignant myeloid diseases to 1-1.5 Mb and preparation of a PAC-based physical map. *Proc. Natl. Acad. Sci. USA.* 94:6948–6953. http://dx.doi.org/10.1073/pnas.94.13.6948

Zhao, J.L., D.S. Rao, M.P. Boldin, K.D. Taganov, R.M. O'Connell, and D. Baltimore. 2011. NF-kappaB dysregulation in microRNA-146a-deficient mice drives the development of myeloid malignancies. *Proc. Natl. Acad. Sci. USA.* 108:9184–9189. http://dx.doi.org/10.1073/pnas.1105398108